Effect of Early Life Stress (ELS) on innate predator odour processing and defensive behaviours in mice

A Thesis

submitted to

Indian Institute of Science Education and Research Pune in partial fulfilment of the requirements for the Master of Science programme

by

Lavanya Ranjan

Indian Institute of Science Education and Research Pune

Dr. Homi Bhabha Road,

Pashan, Pune 411008, INDIA.

Date: March 27, 2025

Under the guidance of

Supervisor: Dr. Nixon M. Abraham,

Department of Biology, IISER Pune

From May 2024 to Mar 2025

INDIAN INSTITUTE OF SCIENCE EDUCATION AND RESEARCH PUNE

Certificate

This is to certify that this dissertation entitled **Effect of Early Life Stress (ELS) on innate predator odour processing and defensive behaviours in mice** towards the partial fulfilment of the MS (by Research) programme at the Indian Institute of Science Education and Research, Pune represents study/work carried out by Lavanya Ranjan at Indian Institute of Science Education and Research under the supervision of Dr. Nixon M Abraham, Associate Professor, Department of Biology, during the academic year 2024-2025.

Dr. Nixon M Abraham

Committee:

Dr. Nixon M. Abraham

Dr. Raghav Rajan

This thesis is dedicated to my parents and my sister – who not only tolerated my numerous antics but also pushed me to always strive for bigger things. This thesis stands as a testament to my mom’s courage and dreams, my father’s love, and my sister’s perseverance in standing by me.

Declaration

I hereby declare that the matter embodied in the report entitled **Effect of Early Life Stress (ELS) on innate predator odour processing and defensive behaviours in mice** are the results of the work carried out by me at the Department of Biology, Indian Institute of Science Education and Research, Pune, under the supervision of Dr. Nixon M. Abraham and the same has not been submitted elsewhere for any other degree

Lavanya Ranjan

Date: 27-03-25

Table of Contents

List of Tables

List of Figures

Abstract

Fox urine odour 2,5-dihydro-2,4,5-trimethylthiazoline (TMT) has been known to produce avoidance and freezing – innate defensive behaviours which are believed to be genetically hard-wired. These behaviours indicate a possible stress response due to elevated serum corticosterone. Notably, early life stress (ELS) in humans as well as animal models has been linked to diverse forms of cognitive and sensory deficits in their adult lives. This is because the early postnatal brain continuously experiences developmental processes such as axonal and dendritic growth, and synaptic pruning. Thus, stress experienced during the early-life period can have drastic impacts on the developing brain. Previously, a study from our lab demonstrated that ELS can cause olfactory learning deficits. However, whether the effects of ELS also manifest into innate behaviours remains unanswered. In this thesis, we investigated the effects of early life stress on innate defensiveness in mice. Exposure to TMT resulted in hyperactivity and lesser freezing of ELS mice compared to normally weaned mice of similar age. Further, significantly lesser c-Fos expression in the olfactory bulb (OB) of ELS mice compared to the normally weaned group in response to TMT implies reduced population activity due to chronic stress. Although the circuitry and molecular mechanisms mediating such changes are still under investigation, unpublished data from the lab suggested the role of OB interneurons in predator odour processing and mediating these defensive responses. Our current work further tweaks the activity of these interneurons to discern their plausible role in predator odour processing and innate defensive behaviours in ELS mice using optogenetics. We report increased mobile time in ELS mice while photoactivating the inhibitory network compared to control animals. These results thus confirm the role of OB inhibitory interneurons in modulating threat perception under early life adversity.

Acknowledgments

The work in this thesis has only been possible due to the innumerable people involved and their critical inputs and guidance. I am grateful to my thesis supervisor Dr. Nixon M. Abraham for his constant mentorship and guidance throughout the project. I have been inspired by his passion and rigorous scientific temper with which he approaches Science. Further, I am thankful to my TAC member Dr. Raghav Rajan for his constructive inputs and insightful perspective in shaping this project.

I am immensely grateful to my mentor Sanyukta Pandey who not only shaped the trajectory of this project, but also motivated me to always explore newer things, in the project as well as in life. I would be forever indebted to her for teaching me so many things and believing in me when things went downhill. I would like to especially acknowledge all the wonderful people of LNCB – Devesh, Debarghya, Kirti, Susobhan, Shruti and Karishma who were always there whenever I needed help with anything, both in and outside lab. Further, I would like to call out all the members of the lab (both past and present), working with whom I have had countless fun-filled days: Mridula, Giri, Ganesh, Alivia, Vaishnavi, Adarsh, Ahmed, Sharvari, Prachi, Kevin, Ananya, Aditi, and Krish. I am grateful to the members of Animal House facility for timely providing me with the animals for my study, Microscopy facility for enabling me to use the resources and IISER Pune for the fellowship and offering me this platform to present my work.

My stay at IISER would never have been so memorable without my incredible friends – Devika, Pulkit, Priyojit, Kamalika, Arpan, Vikas and Ojasvi. I would forever treasure the beautiful time and conversations I have had with you all. I would also like to acknowledge my friends from home: Vaishnawi, Surabhi, Rishi and Shivani. Despite staying far away, they were always there to listen to my misfortunes and lighten my mood. Lastly, my deepest appreciation goes to my parents and sister—without their unwavering support, this academic journey would have never been possible.

Contributions

Contributor name	Contributor role
Dr. Nixon M. Abraham, Sanyukta Pandey	Conceptualization Ideas
Lavanya Ranjan, Sanyukta Pandey	Methodology
Lavanya Ranjan, Sanyukta Pandey	Software
Lavanya Ranjan, Sanyukta Pandey	Validation
Lavanya Ranjan, Sanyukta Pandey	Formal analysis
Lavanya Ranjan	Investigation
Dr. Nixon M. Abraham	Resources
Lavanya Ranjan	Data Curation
Lavanya Ranjan	Writing - original draft preparation
Dr. Nixon M. Abraham, Sanyukta Pandey	Writing - review and editing
Lavanya Ranjan	Visualization
Dr. Nixon M. Abraham, Sanyukta Pandey	Supervision
Lavanya Ranjan, Dr. Nixon M Abraham	Project administration
Dr. Nixon M. Abraham	Funding acquisition

This contributor syntax is based on the Journal of Cell Science CRediT Taxonomy[1].

[1] https://journals.biologists.com/jcs/pages/author-contributions

Chapter 1 Introduction

1.1 The neurobiology of fear

Over the past few decades, considerable effort has been dedicated to unraveling the underlying mechanisms of fear and associated defensive responses elicited against threatening stimuli. 'Fear' in a very broad sense refers to the conscious feeling that one experiences in the face of a survival threat, triggering instinctive physiological and behavioural responses to the perceived danger (Gross and Canteras, 2012; Silva *et al.*, 2016). However, there is considerable debate in the community as to what extent and if non-human animals are capable of experiencing fear, and if it could be paralleled to the human feeling of fear (LeDoux, 2012; Anderson and Adolphs, 2014). Nevertheless, a growing consensus among neuroscientists suggests that decoding the neural circuits driving threat responses in animals and humans holds the key to unraveling the mechanisms of fear (Gross and Canteras, 2012; LeDoux, 2012). Animals including rodents possess a natural instinct of protecting themselves from overt dangers which can elicit innate defensive responses. In rodents, fear-elicited defensive responses could be triggered by a variety of stimuli – they could be predator or aggressive conspecific odour-induced, or could be fear of painful stimuli. Interestingly, these stimuli trigger defensive responses without requiring prior experience or memory of direct harm, thereby carrying an inherent 'negative valence' toward the threat. This form of fear is denoted as "innate fear" (Blanchard and Blanchard, 1989; Silva *et al.*, 2016).

Notably, such defensive responses can also be induced by associating a cue with a threatening stimulus, such as a foot shock, piercing noise, or other aversive stimuli—a phenomenon known as 'fear conditioning' (Gross and Canteras, 2012; Fadok *et al.*, 2017; Wang *et al.*, 2024). A growing body of literature suggests that innate fear—whether triggered by predators or conspecifics—and conditioned fear and memory are processed by distinct, non-overlapping circuits, each regulating passive and active defensive responses in unique ways (Gross and Canteras, 2012; Isosaka *et al.*, 2015; Efrat Jacob, 2023; Khalil *et al.*, 2023).

A study by Morrow et al., had shown that in mice, serum corticosterone and central dopamine metabolism were significantly elevated in the central amygdala and medial pre-frontal cortex (mPFC) upon exposure to predator odour. However, in the case of foot-shock based fear stimulus, they were elevated in mPFC and Nucleus accumbens (both core and shell regions, NAc and NAs, respectively), indicating that innate and conditioned stimuli are processed differently (Morrow *et al.*, 2000).

1.1.1 Predator odour TMT acts as an innate stressor

Rodents rely heavily on odours as navigational tools, helping them locate food, engage in social interactions, find mates, and detect lurking dangers. These innate behaviours surface spontaneously in naïve animals, and require no prior learning or experience, hinting that the underlying neural circuits are genetically hardwired (Kobayakawa *et al.*, 2007). When it comes to threat detection, the ability to instantly sense a predator's presence is crucial for survival. Predators like cats, foxes, and ferrets release specific chemical cues called **kairomones** (Matsukawa *et al.*, 2022). These interspecies signals, unfavourable to the predator itself, ignite rapid fear and stress responses in rodents. While these responses are essential for survival, their dysregulation can lead to altered behavioural states, including anxiety, despair-like symptoms, phobias, and post-traumatic stress disorder (PTSD) (Tyler *et al.*, 2020). Behaviourally, kairomones-induced acute stress can elicit either active or passive defensive responses. While

active displays manifest as fight-flight responses (attack or avoidance), passive responses can be a display of freezing. And, interestingly, all of them indicate anxiety (Matsukawa *et al.*, 2022). Traditionally, avoidance or escape is measured by quantifying the escape/flight frequency, escape velocity, jump frequency, and calculation of aversion/flight score (Fadok *et al.*, 2017; Wang *et al.*, 2024). However, freezing refers to the complete cessation of all motor activities, except respiration and is quantified by measuring immobility (Root *et al.*, 2014; Florido *et al.*, 2024).

A key predator odour is 2,5-dihydro-2,4,5-trimethylthiazoline (TMT), a compound found in fox faeces (Fendt *et al.*, 2018). In rodents, TMT functions as an innate stressor by activating their autonomic nervous system (ANS) as well as the endocrine system. The ANS enables them to produce a rapid, and short-term response while the endocrine brings about a sustained response. Further, an acute exposure to TMT brings about a distinct pattern of activation in different brain areas, which is different from those evoked by conditioned-fear stimulus (Matsukawa *et al.*, 2022). Like other volatile odorants, TMT is sensed by the olfactory subsystems in the periphery. TMT also possesses trigeminal sensitivity at higher concentrations. Reports on olfactory sensory neuron ablation and bulbectomy alleviating TMT-induced defensive responses in rodents demonstrate the importance of pre-cortical neuronal circuits in threat perception and associated behavioural states (Hacquemand *et al.*, 2010).

Therefore, a broad outline about the rodent olfactory system, odour processing and associated circuits for innate fear is enumerated below.

1.1.2 Olfactory subsystems, odour processing and predator-odour induced innate fear circuitry

The olfactory system comprises four major subsystems which bear the olfactory sensory neurons (OSNs) – the main olfactory epithelium (MOE), the vomeronasal organ (VNO), the septal organ of Masera (SOM), and the Grüneberg ganglion (GG) (Figure 1). While the MOE sends its projections to the main olfactory bulb (MOB), projections from the VNO transmit signals to the accessory olfactory bulb (AOB) (Barrios *et al.*, 2014). SOM, located at the ventral end of the nasal septum projects to a few glomeruli in the MOB (Ma *et al.*, 2003; Tian and Ma, 2004). Lastly, GG situated at the rostral end of the nasal cavity projects caudally to necklace glomeruli (NG) at the anterior part of the AOB (Fuss *et al.*, 2005; Mamasuew *et al.*, 2008). Of the four subsystems, TMT activates three of them: GG, MOE, and VNO. Further, about 70% of the GG neurons are activated while 10-25% of MOE and <10% of VNO neuronal population are activated in response to TMT (Brechbühl *et al.*, 2013).

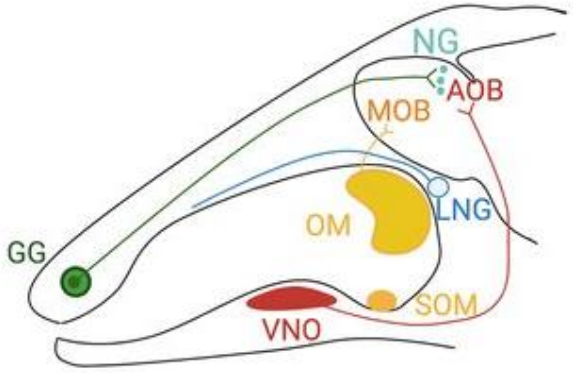

Figure 1 Schematic illustrating the mouse olfactory subsystems.
Olfactory mucosa (OM) harbours the main olfactory epithelium (MOE), which projects to the main olfactory bulb (MOB). The vomeronasal organ (VNO) projects to the accessory olfactory bulb (AOB), while the Grüneberg ganglion (GG) projects to the Necklace glomeruli (NG) Adapted from (Abaffy et al., 2023).

Odour detection is initiated when odorant molecules in our environment bind to the odorant receptors present on olfactory sensory neurons (OSN) lining the main olfactory epithelium in the nasal cavity. These odorants bind to specific G-protein coupled receptors on OSNs and transduce a cAMP-based transduction cascade, which eventually converts the chemical information to an electrical signal. This is further transmitted to the OB and, eventually to higher cortical areas (Boccaccio *et al.*, 2021). A schematic representation of the basic model of the olfactory bulb network, and various cell types is illustrated in Figure 2.

In the olfactory bulb (OB), axons from OSNs in the olfactory nerve layer (ONL) traverse through the cribriform plate to synapse in a neuropil-like structure called glomeruli, in the glomerular layer (GL). Each OSN expresses only one type of olfactory receptor (OR), which can bind to multiple odorants while a group of receptors recognise each odorant molecule, except for the MS4 sensory neurons that are shown to harbour many receptors (Greer *et al.*, 2016). Although the GL bears several thousand glomeruli that perforate the OB, OSNs expressing the same type of odorant receptors converge in a few distinct glomeruli, thus essentially mapping the odour that activates them – a phenomenon known as combinatorial coding (Malnic *et al.*, 1999).

Histologically, the OB could be divided into multiple distinct layers, each studded with morphologically distinct neuronal cell types. Based on the neuronal cell body that inhabits these cell layers, they are divided into:

a. **Glomerular layer (GL):** houses the juxtaglomerular cells, which, on the basis of morphology are sub-divided into the periglomerular (PG) cells, external tufted (ET) cells, and superficial short-axon cells (SAC).
b. **External plexiform layer (EPL) and Mitral cell layer (MCL):** house the cell bodies of tufted cells (TC) and mitral cells (MC), respectively.
c. **Granule cell layer (GCL):** bears axon-less interneurons called granule cells (GC).

Mitral and tufted cells, known as projection neurons, are the sole cell types that extend their axons into the olfactory cortex (OC), making them the primary cells for propagating odour signals. Each of these neurons projects a single primary dendrite into a specific glomerulus, where they receive synaptic inputs from OSN axons and establish reciprocal synapses with synapses of PG cells. Additionally, their secondary dendrites extend across the external plexiform layer (EPL), where they engage in dendrodendritic reciprocal synapses with granule cell dendrites.

Beneath the EPL, the internal plexiform layer (IPL) and the granule cell layer (GCL) predominantly house granule cells, which extend apical dendrites into the EPL. The soma of tufted cells, located in the EPL, and mitral cells, found in the mitral cell layer (MCL), receive incoming signals, which are then transmitted horizontally via secondary dendrites in the EPL. As this signal propagates laterally, it encounters inhibition from granule cell dendrites, which, through dendrodendritic synapses, suppress the activity of neighboring mitral and tufted cells. This mechanism, known as lateral inhibition, refines odor signal processing by modulating neuronal activity within the circuit (Nagayama *et al.*, 2014).

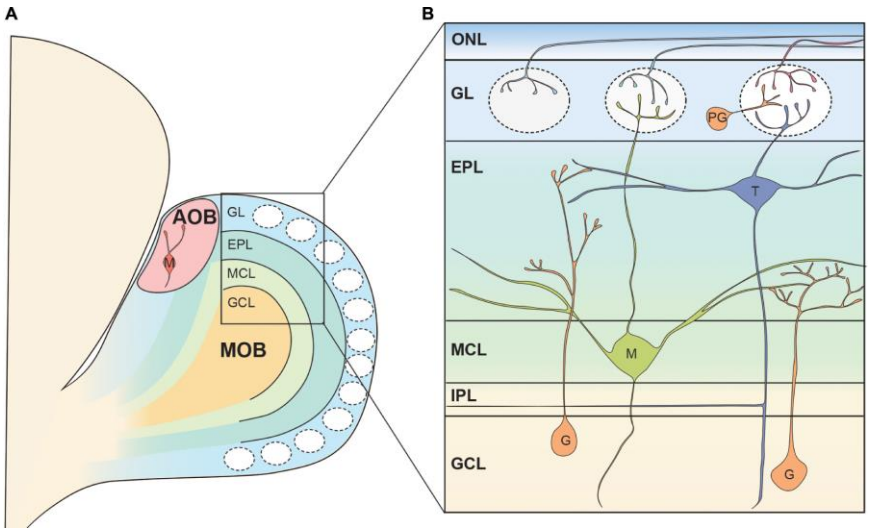

Figure 2 The odour processing circuitry.
The olfactory bulb (OB) presents a layered structure with each layer studded with morphologically distinct cells.
A) Saggital section of the OB, B) Distinct cell types inhabiting each layer. Taken from (Imamura et al.*, 2020).*

1.1.3. Predator-odour induced fear circuitry

Numerous studies have indicated that the fear circuitry is remarkably intricate, consisting of multiple independent pathways that orchestrate different defensive responses and distinct forms of fear. In the case of conditioned fear, flight, and freezing are mediated by distinct CeA (central amygdala) interneurons, engaged mutually in reciprocal inhibition – such that the choice of the adequate behavioural response relies on the dynamic competitive interactions between the two populations (Fadok *et al.*, 2017). While a lot remains to be uncovered in terms of the neural underpinnings of the innate fear circuitry, two such pathways are discussed below.

a. OB-CoA mediated circuitry

Predator odour is primarily detected by two subsystems of the olfactory system: by MOE which majorly responds to volatile cues (including odours like TMT), and by VNO which responds to non-volatile cues (Takahashi, 2014; Pardasani *et al.*, 2021; Marathe and Abraham, 2024). MOE inputs relay these information to the projection neurons in the posterior dorsal and lateral olfactory bulb (Kobayakawa *et al.*, 2007), which eventually send their inputs to the cortical amygdala (CoA) (Miyamichi *et al.*, 2011). Alternatively, signals from the accessory olfactory pathway (by VNO) are relayed to the MeA (medial amygdala) (Gross and Canteras, 2012). Further, recent studies have also implicated GG in the detection of con-specific alarm pheromones and predator-odours that bear a structural similarity to these pheromones (Takahashi, 2014). Much about the role of cortical areas arises from the optogenetic studies by Root et al. – which demonstrated that inhibition of OB-CoA pathway or just neuronal population in CoA lead to a reduction in freezing behaviour by 20% in response to TMT, implicating an important role of CoA in mediating odours of threatening valence (Root *et al.*, 2014).

b. OB-DP mediated circuitry

However, given the low reduction in freezing due to CoA silencing, a recent study by Wang et al., argued the presence of another amygdala-independent OB-dorsal peduncular cortex (DP) mediated pathway for relay of TMT-evoked information to cortical areas. Opto-silencing of DP leads to a 60% reduction in flight behaviour and 40% reduction in freezing during TMT exposure. Their findings suggest that mitral and tufted cell outputs from the OB relay signals

to calmodulin-dependent protein kinase II-expressing (*CaMKII*$^{+}$) pyramidal neurons in the dorsal peduncular cortex (part of the olfactory cortex). These, in turn, connect to cholecystokinin-expressing (*Cck*$^{+}$) neurons in the superior lateral parabrachial nucleus (PBNsl). Further projections to tachykinin 1-expressing (*Tac1*$^{+}$) neurons in the parasubthalamic nucleus (PSTh), ultimately drive flight behaviour and, to a lesser extent, freezing responses in mice (Wang *et al.*, 2024). A schematic representing their model of TMT-odour driven fear and anxiety is represented in Figure 3.

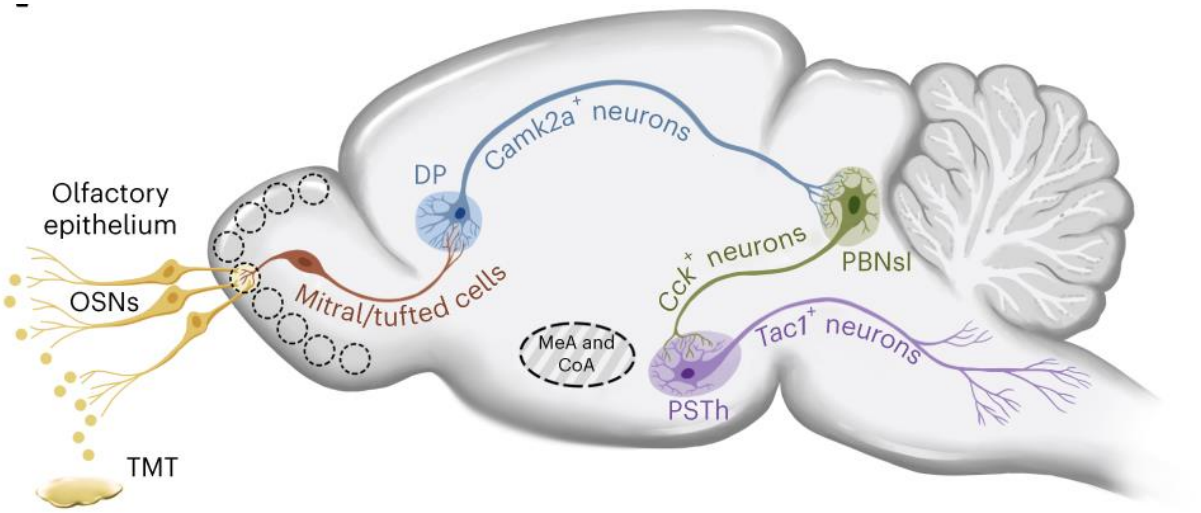

Figure 3 Model representing the neuronal circuitry for TMT-odour driven flight behaviours in rodents. Adapted from Wang et al., 2024.

Of note, immuno-histochemical evidence from their study also demonstrated that the mitral-tufted cell projections from the main olfactory bulb to DP or amygdala are morphologically distinct indicating that these two circuitries might be working in tandem to elicit innate defensive responses in mice.

It is interesting to note that, although the pathways that relay olfactory signals from the sensory organs to both cortical and subcortical olfactory centres have been well-studied (Ghosh *et al.*, 2011; Miyamichi *et al.*, 2011; Sosulski *et al.*, 2011), the specific pathways responsible for triggering innate odour responses via the OB-CoA mediated pathway are yet to be uncovered.

1.2 Effect of stress on cognitive and innate behaviours

As elegantly put forward by McEwen et al. stress is not just a multifaceted phenomenon at the cell and circuit level, it's also equally complex and variable at the behavioural level (Joëls and Baram, 2009; McEwen *et al.*, 2015). While a moderate amount of stress is beneficial in improving performance for some tasks, prolonged, chronic stress can lead to dysfunctional responses, which ultimately can lead to deleterious consequences (Shonkoff *et al.*, 2009; Ryu and De Marco, 2017).

A number of studies indicate that acute, uncontrollable stress can impair decision-making in humans (Soares *et al.*, 2012; Liu *et al.*, 2024), and rats (Jones *et al.*, 2009; Laino Chiavegatti and Floresco, 2024). Notably, a study by Jones et al. shows that rodents can be engaged in a water foraging choice task where they are trained to forage for equal amounts of water (as a reward) in the left and right arms of a maze. However, when the water amount is tripled – the stressed group mice (subjected to acute stress of 60 minutes of restraint and tail shocks), are

consistently unable to bias their response towards a larger water reward in comparison to controls that always chose the larger reward. This indicates the adverse effects of stressful conditions on decision-making (Jones *et al.*, 2009). This notion is supplemented by yet another study that examined the balance between goal-directed and habitual behaviour, and found an increase in habitual behaviours in stressful conditions. They suggest that this balance allows for adaptability in the decision-making process which enables one to weigh-in the consequences in a dynamic scenario. While goal-directedness enables one to assess and eventually choose a favourable situation, habitual behaviours enable one to complete routine tasks drawing on past successes (Giovanniello *et al.*, 2025).

Traditionally, Yerkes-Dodson law proposes that the level of acute stress and cognition follow an inverted U-shaped relationship (Chaby *et al.*, 2015; Corbett, 2015). This is evidenced by some studies that demonstrate that physiological manifestations of acute versus chronic stress are non-linear (McEwen *et al.*, 2015; Ryu and De Marco, 2017). However, whether such a relationship also exists between stress and innate behaviours remains unanswered.

1.2.1 Chronic stress and early life adversity

The early postnatal period is a pivotal period in the course of brain development, marked by key processes such as axonal and dendritic growth, as well as synaptic pruning. Stress encountered during this critical period can drastically impact normal brain development and lead to detrimental responses to stressors. (Shonkoff *et al.*, 2009; Chen and Baram, 2016).

Early-life stress (ELS) or early-life adversity (ELA) refers to exposure to adverse environmental conditions, including parental separation, substance abuse, violence, malnutrition, and neglect during this period. Previously, ELS mice have been shown to have heightened levels of anxiety and disrupted social behaviour (Wei *et al.*, 2012; Bondar *et al.*, 2018; Breton *et al.*, 2024). Notably, numerous studies in the past have linked stressful experiences in infancy to higher probabilities of developmental and neuropsychiatric disorders in humans and animal models (Mueller *et al.*, 2010; Carr *et al.*, 2013; Chen and Baram, 2016; Nishi, 2020; Smith and Pollak, 2020; Lee and Jung, 2024).

In the context of pain perception, ELS has been shown to increase mechanical as well as thermal hypersensitivity in mice, as measured by decreased latencies in paw withdrawal to heat and pressure stimuli, indicating its adverse effects on the central nervous system to mount reflexive behaviours (Nishinaka *et al.*, 2015; Fuentes and Christianson, 2018). Moreover, a study from our lab had demonstrated that ELS can cause olfactory learning deficits (Pardasani *et al.*, 2023). However, whether the effects of ELS also manifest into innate behaviours remains unanswered.

To address this gap, we aimed to utilise a behavioural paradigm in which ELS mice are introduced to the predator odour TMT. This project aims to explore how early-life stress influences innate processing of predator odours and the defensive behaviours associated with them, using TMT exposure in young adulthood as a model for stress induction.

Further, we have also tried to ameliorate the adverse effects of ELS by providing environmental enrichment (EE) to a subset of ELS mice and then understand how their behavioural responses are shaped.

1.2.2 Models of generating ELS

A number of models exist for generating ELS in rodents (Tran and Gellner, 2023), however the widely accepted ones are:

a. Early weaning (EW): involves separation of the pups from the dams at P14 resulting in a loss of maternal care and lactation (Pardasani *et al.*, 2023).
b. Infant Maternal Separation (IMS): involves separation of pups from dams for a few hours every day (~3H), ranging from P2-P22, resulting in disrupted and erratic maternal care (Lee and Jung, 2024).
c. Limited Bedding and Nesting (LBN) paradigm: includes limited access to bedding and nesting for the dams in the early-postnatal period of her pups, resulting in fragmented, chaotic and unpredictable maternal care (Gallo *et al.*, 2019).

We have employed EW to induce ELS as it has been reported to disrupt the hypothalamic-pituitary-adrenergic (HPA) axis and induce chronic stress by elevation of ACTH and glucocorticoids (McEwen *et al.*, 2015; Lee and Jung, 2024). Moreover, to understand how olfactory inputs from the periphery contribute to innate defensive responses, it is essential to explore the connections and their cross-talk with the stress circuitry. A brief description is outlined below.

1.2.3 Olfactory information processing and the activation of stress-related circuitry

Olfactory information from mitral and tufted cells in the OB projects to five distinct regions in the following order: anterior olfactory nucleus (AON), piriform cortex (anterior and posterior, APC and PPC), olfactory tubercle (OT), cortical Amygdala (Amy), and entorhinal cortex (EC) (Root *et al.*, 2014). From here, bidirectional innervations lead to Hippocampus and Amygdala which can activate the Bed Nucleus of Stria Terminalis (BST), which can further activate the hypothalamic-pituitary-adrenergic (HPA) axis. The pituitary gland triggers the production and release of adrenocorticotropic hormone (ACTH), which travels through the bloodstream to the adrenal cortex. In response, the adrenal cortex produces and releases glucocorticoids (GCs) such as corticosterone which eventually mounts the physiological responses by activating the sympathetic nervous system, thus initiating the body's stress response (Lee and Jung, 2024). A schematic of the associated circuitry is illustrated in Figure 4.

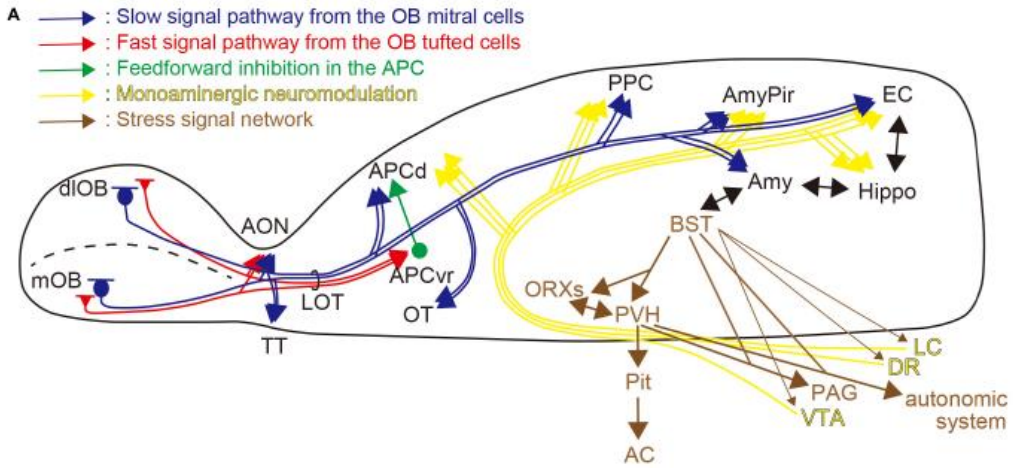

Figure 4 Overview of the olfactory information processing and stress-related networks.

Blue represents the feedforward excitatory signal from projection neurons of olfactory bulb (OB). This signal is further transmitted to Hippocampus (Hippo), Amygdala (Amy), & Bed Nucleus of Stria Terminalis (BST) which activates Hypothalamus (PVH and ORXs). This leads to activation of HPA axis. Taken from Matsukawa et al., 2022.

It is interesting to note that, although the pathways that relay olfactory signals from the sensory organs to both cortical and subcortical olfactory centres have been well-studied (Ghosh *et al.*, 2011; Miyamichi *et al.*, 2011; Sosulski *et al.*, 2011), the specific pathways responsible for triggering innate odour responses are yet to be uncovered. Additionally, whether chronic stress state alters the notion of perceived threat and thereby the innate defensiveness remains heavily unexplored. Therefore, this thesis specifically delves into how defensive responses elicited due to innate 'fear' in response to a predator odour are affected by chronic stress – using mouse as a model system.

Chapter 2 Materials and Methods

2.1 Experiment 1: Behavioural characterization of ELS, NW and ELS-EE mice in response to PBS, AA and TMT

2.1.1. Animals used

For behavioural characterisation, a total of 27 C57BL/6J male mice (from Jackson Laboratories) were utilised for the study. These were divided into three groups (Figure 7B):

1. Normally weaned mice (NW): included a total of 10 mice which were weaned at post-natal day 21 (PND21/ P21) and housed in standard individually ventilated cages (IVC).
2. Early-life stressed mice (ELS): These were procured as pups on post-natal day 14 (PND14/ P14), and housed in IVC cages until experimental age (8-11 weeks/ P56 onwards, 7 mice).
3. ELS-Environmentally enriched (ELS-EE) mice (n=10 mice): These were weaned at PND 14 and subjected to early-life stress until P21, following which they were transferred to a custom-built cage (90 cm X 60 cm X 45 cm) for environmental enrichment until experimental age (P56 onwards). A schematic illustrating the timeline for rearing and experiments for the three cohorts of mice is illustrated in Figure 5.

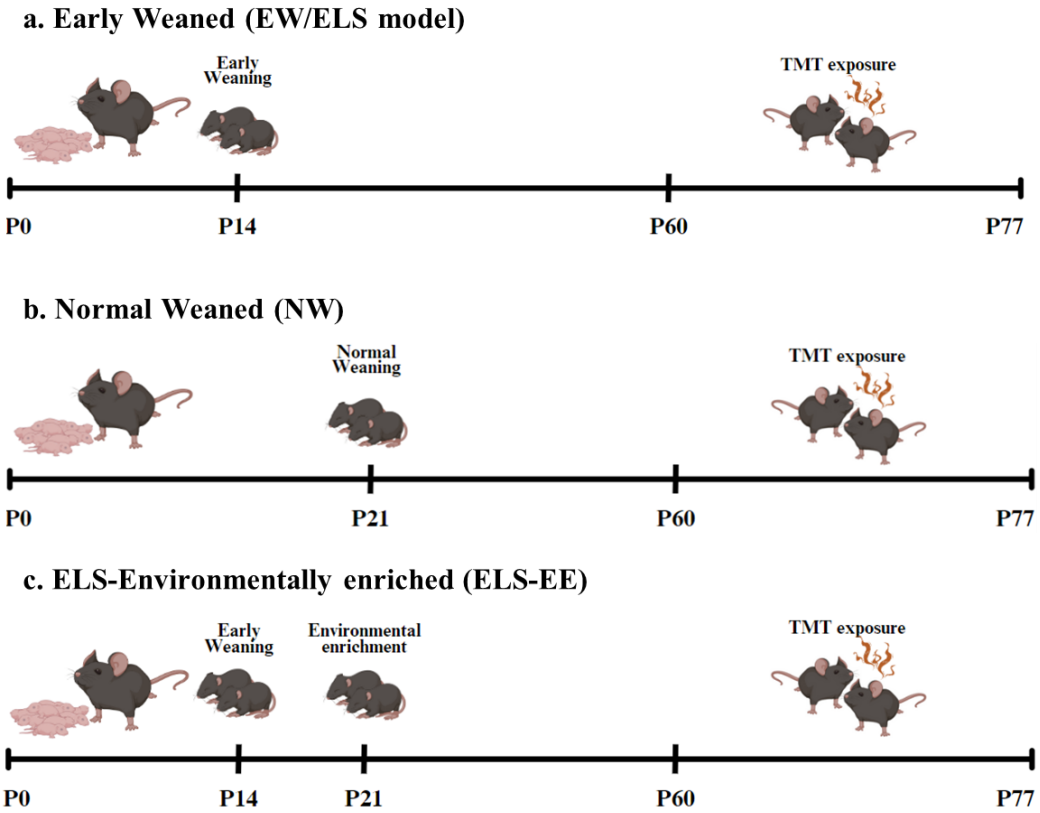

Figure 5 The timeline followed for rearing and experimentation for ELS, NW and ELS-EE mice. Image created using BioRender.

For optogenetic experiments, a total of 20 mice were utilised. These belonged to the early-life stressed (ELS) set. These were further divided into three sub-groups: 7 Gad2 Cre x ChR2, 7 Gad2 Cre x EYFP and 6 Gad2 Cre x ArchGFP. These mice were procured at their respective PND 14 and were subsequently housed in standard IVC cages until they attained the experimental age of 8 weeks.

A cupping technique was used to handle the animals for the entirety of the experimentation to avoid anxiety and any bias due to handling itself. Both EW and EE paradigms were adapted from previous works of Meenakshi Pardasani and Eleanor McGowan in the lab (Pardasani *et*

al., 2023). All animals were maintained on a twelve-hour light/dark cycle and housed in individually ventilated cages (IVC) in cohorts of 2-6 in a temperature and humidity-controlled environment, unless otherwise noted. Further, all the experiments and procedures performed were in accordance with the Institutional Animal Ethics Committee (IAEC), IISER Pune and the Committee for Control and Supervision of Experiments on Animals (CCSEA), Government of India.

2.1.1.1. Protocol for early weaning

As described by Pardasani et al., to induce ELS due to early weaning, P14 pups post-weaning were housed in a cage with new bedding and limited new nesting material. Food pellets were provided in the form of slurry and were supplemented with a special feed (rich in protein and carbohydrate, until P21). Both slurry and water were kept in petri-plates, and provided *ad libitum*. To avoid death due to hypothermia in the initial days, intermittent heating was provided by a heating pad for 20 minutes, twice every day from P14-P18.

2.1.1.2. Environmental enrichment to ELS mice

To counter the stress created due to ELS, a custom-built cage made up of clear acrylic sheets (90 cm X 60 cm X 45 cm) was used for housing the third set of mice. This cage had supplies for sensory (olfactory and tactile), motor and, cognitive enrichment of the animals. It was connected to the existing IVC system using 3 inlets and 3 outlets for entry of clean and exit of foul air. The cage was divided into two levels: upper and a lower level. The lower level had 2-3 plastic toys (running wheels and dishes for motor activities), a wooden hut and tunnel, and a wooden chewing toy. Further, 2 small spice boxes with few holes for odour diffusion were placed for olfactory enrichment. The spices were replaced every alternate day with natural odorants (cinnamon, clove, cardamom, coco-chips, bay leaf, almonds, and dried fruit). For somatosensory enrichment, Lego pieces, and cubes with textured surfaces were used. Food and water were provided *ad libitum* in the form of pellets and via a free-standing water bottle, respectively. The bedding and nesting material was changed weekly, and the toys were rearranged to prevent habituation and to alleviate their explorative nature.

For enhancing cognitive development, the upper level had a maze built out of Lego pieces which was changed every week to provide novelty. In addition, a Lego staircase was placed to aid in mobility between the upper and lower levels. Figure 6 below showcases the enrichment cage setup utilised for the study.

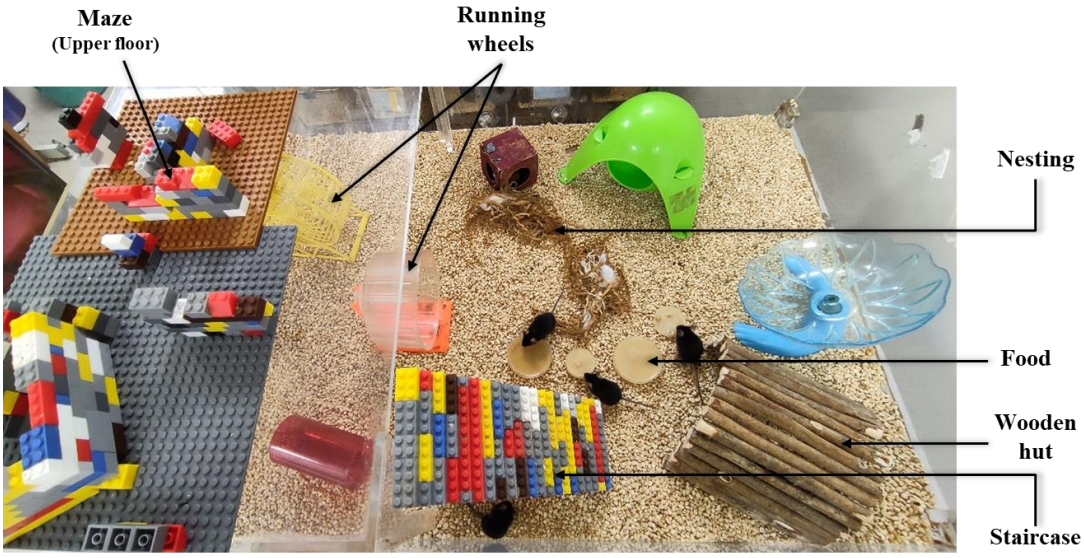

Figure 6 The environmental enrichment (EE) setup with ELS mice at PND14.
It includes a number of toys, running wheels / dish, burrowing huts and tunnels, and a Lego staircase that connects to the upper level of the cage. The upper level has a Lego maze for cognitive enrichment. A few odour boxes are also kept for olfactory enrichment (not shown).

2.1.2. Experimental Setup

All experiments were carried out in a small, custom-made plexiglass chamber (illustrated in Figure 7A). The chamber consisted of a cylindrical enclosure (diameter and height = 13 cm) with a circular base and a transparent lid (diameter = 13 cm). This chamber was further placed within an opaque rectangular box made up of black, non-reflective acrylic sheets (dimensions: 63 cm × 45 cm × 43 cm; (L×B×H)) to prevent any disturbances to the animal due to the external surroundings.

Odour delivery in the chamber was achieved by pipetting a small amount (10 µl of the respective diluted odour) on a kimwipe which was taped to the interior of the lid during the experiments. The kimwipe was taped at the centre to ensure uniform distribution of odour throughout the chamber. Further, during the experiments, the arena was cleaned with distilled water before introducing each animal.

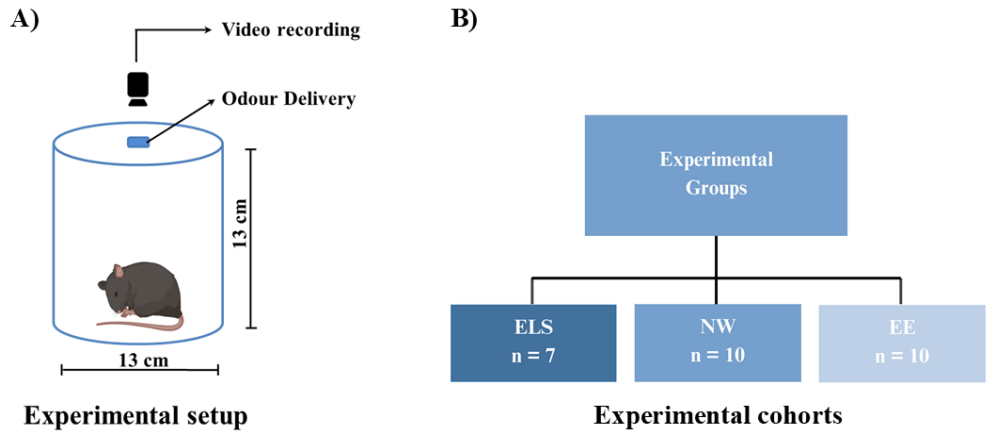

Figure 7 The experimental chamber and groups of mice utilised.
Panel A illustrates the experimental chamber utilised for habituation and odour exposure sessions. Panel B denotes the experimental cohorts utilised in the study.

2.1.3. Behavioural Testing and Paradigm

2.1.3.1. Tests for anxiety-related behaviours

All animals were subjected to a standard battery of tests to assess their anxiety and stress levels. Further, videos were recorded for each one of them for subsequent behavioural analysis. A one-day gap was provided between each of the test.

1. Open Field Test (OFT)
   First developed by Hall in 1934 (Hall, 1934), OFT involves introduction of the animals into a large, square arena for a definite period of time while their exploratory behaviour is recorded. Typically, rodents display thigmotactic behaviour – spending a greater amount of time near the walls of the arena with relatively lesser centre approaches (Lezak *et al.*, 2017; Tucker and McCabe, 2021).

   Each mouse was allowed to enter an open field arena (60 cm x 45 cm), where their behaviour was recorded for 10 minutes. Further, their behaviour was analysed by Noldus Ethovision to calculate the time spent in the central area and the corners of the arena.

2. Elevated Plus Maze (EPM) assay
   The EPM apparatus bears a pair of open arms and closed arms (each 20 cm in length), oriented in a plus-shaped fashion with a central square space (5cm x 5cm). The entire arena is elevated 50 cm above the ground. Contrary to OFT, the stressor here is the absence of thigmotactic cues in the open arms of the arena (Tucker and McCabe, 2021).

Each mouse was introduced into the central space while facing the open arms, and then allowed to explore. Their behaviour is recorded for 5 minutes and the time spent in open versus closed arms is calculated, as well as the number of entries made.

2.1.3.2. Behavioural Paradigm

The behavioural paradigm comprised both habituation as well as odour exposure sessions (Figure 8), lasting for a period of 7 consecutive days. These are detailed below:

a. Habituation sessions
   To avoid stress and any inadvertent bias due to a novel environment, we subjected the animals to four sessions of habituation in the experimental arena, on four consecutive days to facilitate acclimatization. During habituation, the mice were introduced to the arena, after which the lid was closed promptly. Each session lasted for 10 minutes after which the animal was replaced to its home cage. The arena was cleaned with distilled water after each animal to remove any olfactory cues to the subsequent animal.

b. Odour exposure sessions
   Post habituation, each animal was subjected to three odorants sequentially to assess their behaviour in response to different stimuli. These included an odourless chemical Phosphate Buffer Saline (PBS), an odour with pleasant valence Amyl acetate (AA) (Root *et al.*, 2014), and another odour with negative valence Trimethylthiazoline (TMT) (Root *et al.*, 2014). Odour exposure was performed in the following order:
   i. PBS exposure (10µl): 1x PBS, pH 7.4
   ii. Amyl acetate odour (AA, 10µl): a pleasant, fruity smell, diluted 1% (v/v) in mineral oil (liquid paraffin)
   iii. 2,5-dihydro-2,4,5-trimethylthiazoline (TMT, 10µl): predator odour, diluted 1% in 1x PBS (v/v).

   Each odour exposure session lasted for 10 minutes, in which respective odour was administered using a Kim wipe attached to the centre of the lid on the interior side of the chamber. Behavioural recordings at 25 fps were captured from an overhead perspective to ensure a clear view of the animals' movements without obstructions. This was undertaken for subsequent behavioural analysis of the 10-minute odour duration. The recordings were saved in the MTS file format.

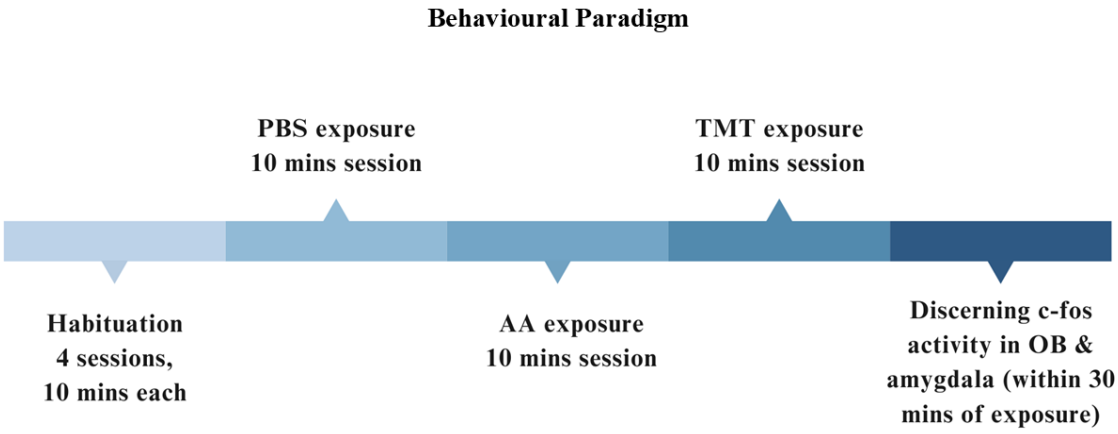

Figure 8 Illustration depicting the sequence of habituation and odour exposure sessions.

2.1.4. Trans-cardial perfusion and brain dissection for Immuno-histochemical analyses

C-Fos, a proto-oncogene, becomes expressed in specific neurons upon depolarization. Its protein product can be identified through immunohistochemical methods, which enables the use of c-Fos as a reliable marker to map neuronal activity across the neuraxis following peripheral stimulation. A number of studies have mapped the expression of c-Fos in response to different natural odours (Bullitt, 1990; Pantazopoulos *et al.*, 2011; Bepari *et al.*, 2012; Lara Aparicio *et al.*, 2022).

In order to study neuronal activity pattern and the role of associated olfactory processing areas, 3 randomly chosen animals each from NW, ELS and EE experimental groups were perfused to visualise c-Fos expression within 30 minutes of predator odour exposure. Their brains were dissected out and 50 μm-thick coronal sections of olfactory bulb were obtained and processed further for immuno-histochemistry (IHC). The protocol for c-Fos staining was followed as detailed by other works from the lab (Pardasani *et al.*, 2023; Mahajan *et al.*, 2024; Marathe and Abraham, 2024). Representative images for c-Fos positive cells in the OB of normally weaned group are shown in the respective results section.

2.1.4.1 Detailed procedure for dissection, fixation and further processing of the brain tissue

a. Trans-cardial perfusion using 30 millileters of 1X Phosphate-buffered saline (PBS) followed by 30 millileters of 4% (w/v) Paraformaldehyde (PFA) to clear off blood from all the tissues was performed. Following this, the brains of the mice were dissected out and incubated in 4% PFA overnight at 4°C.

b. The next day, PFA was drained off and the brain was immersed in 30% sucrose for 24-48 hours at 4°C for cryo-preservation.

c. For cryotome sectioning, the tissue was embedded in thin blocks of optimal cutting temperature (OCT) medium, and then sectioned at -22°C in Leica Cryostat CM1860V. 50 μm-thick free-floating sections of the OB and amygdala were collected in 24-well plates and 6-well plates containing 1x Tris-buffered saline (TBS), respectively.

2.1.4.1.1. Immuno-histochemistry (IHC)

The detailed protocol followed for c-Fos staining is enumerated below:

a. Each of the sections were subjected to prior washing (3x times) with 1% TBST (tris-buffered saline with Triton X-100) for 10 minutes to maintain a constant pH of 7.4 and permeabilize the membrane.
b. To these sections, blocking solution was added: 7.5% normal goat serum (NGS) and 2.5% bovine serum albumin (BSA) in 0.5% TBST. The sections were kept for 2 hours at room temperature.
c. Next, the sections were incubated with primary antibody (rabbit anti-c-Fos diluted 1:750 in blocking solution), overnight at 4°C.
d. 0.1% TBST washes, thrice, for 15 minutes each were given the following day to remove excess of primary antibody.
e. Further, they were incubated with secondary antibody (Alexa Fluor goat anti-rabbit 488, diluted 1:1000 in blocking solution) for 2 hours in dark conditions at room temperature.

f. Sections were then washed (3x times) with 0.1% TBST for 15 minutes each to remove excess of secondary antibody and then counter-stained with DAPI (4',6-diamidino-2-phenylindole), diluted 1: 750 in 1x PBS for 10 minutes, in dark. Subsequently, a 30s 1x PBS wash was performed to wash off excess DAPI.
g. Finally, they were mounted on glass slides using Vectashield anti-fade mounting medium.

2.1.4.1.2. Confocal imaging and quantification of c-Fos positive cells

All imaging was performed on Leica confocal SP8 microscope. For c-Fos quantification, a custom workflow in Huygens professional software was utilised. A 3D ROI was initially defined, and all objects in the ROI within it were counted. Further, filtering was performed to remove all noisy objects less than 500 voxels. All images were processed using similar settings with only minor adjustments to the threshold. After automated counting of the cells, all cells with intensities higher than 1500 voxels (which would arise due to presence of multiple clumped cells) were manually examined in the 3D ROI to discern the true number of cells in the clumps. Quantification was performed for 3 animals with a minimum of 3-5 sections per animal. Further, 4-5 ROIs per section were taken encompassing the entire coronal section.

2.1.5 Behavioural analysis Pipeline

2.1.5.1 Pilot behavioural analysis using Bonsai

Bonsai is an open-source software which can be extensively used for video-tracking and analysis (Lopes *et al.*, 2015; Lopes and Monteiro, 2021). We have used a custom-designed workflow for tracking the position of the centroid (as x, y coordinates) over number of frames (as a proxy for time) in each video of a mouse in our enclosed odour exposure arena (illustrated in Figure 9).

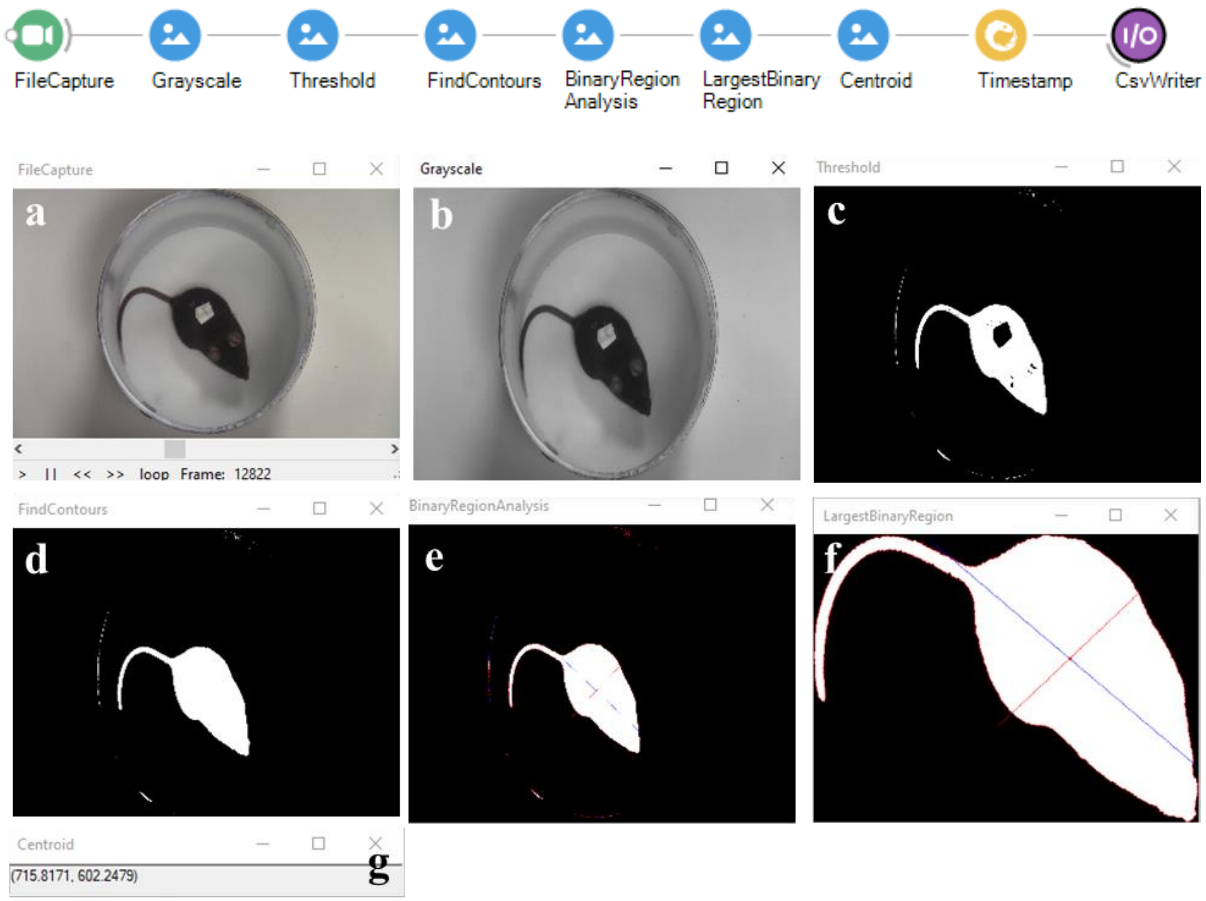

Figure 9 Bonsai workflow and representative images showing the tracking of centroid of mouse.
(Top) A custom-designed Bonsai workflow outlining the image processing pipeline designed to analyze visual data and track movement of the mice. (Bottom) a-g shows the functions of the various nodes as visualised. The centroid of largest binary region (mouse) is used for calculation of mobile vs stationary states.

After converting the input video (Figure 9a) to grayscale (Figure 9b), binary invert mechanism is used to convert pixels into black or white based on a chosen intensity threshold (Threshold node, Figure 9c). Once the contours are fine-tuned (Figure 9d), the arena is analysed for distinct objects by the Binary Region Analysis node (Figure 9e). Next two nodes ensure that the centroid (geometric centre) of the largest object is computed which is exported as x-y coordinates along with timestamp into a csv file (Figure 9e-f).

These x-y coordinates were then used to calculate Euclidean Distance of the position vector which essentially could be approximated to velocity of the centroid considering equal time intervals (40ms) between consecutive x-y coordinates. By utilising a thresholding parameter, we could classify mobile versus stationary states of the mouse. If velocity is below the threshold, the mouse is classified as stationary in that particular frame; otherwise, it's classified as moving. All analysis post-Bonsai video analysis was carried out using custom-written Python scripts and Graphpad Prism 9.5.

2.1.5.2. Pose-estimation using DeepLabCut

Traditionally, behavioural annotation and analysis have mostly been performed manually. This approach is not only time-consuming and labour-intensive, but also inefficient and highly variable. We have employed an open-source software called DeepLabCut (Mathis *et al.*, 2018; Lauer *et al.*, 2022) (DLC) to analyse and quantify different behaviours during odour exposure

of animals. Our pipeline was inspired by similar analyses in crickets and in rodent fear conditioning paradigms (Chanthongdee *et al.*, 2024; Hayakawa *et al.*, 2024). We included the identification and quantification of three different behaviours – exploration, grooming, and freezing.

DeepLabCut employs a convolutional neural network (CNN)-based supervised learning framework to automatically identify and label key anatomical landmarks on mice. The extracted x-y coordinates of these keypoints enable precise, quantitative analysis of body posture and movement. The current DLC workflow is illustrated below in Figure 10.

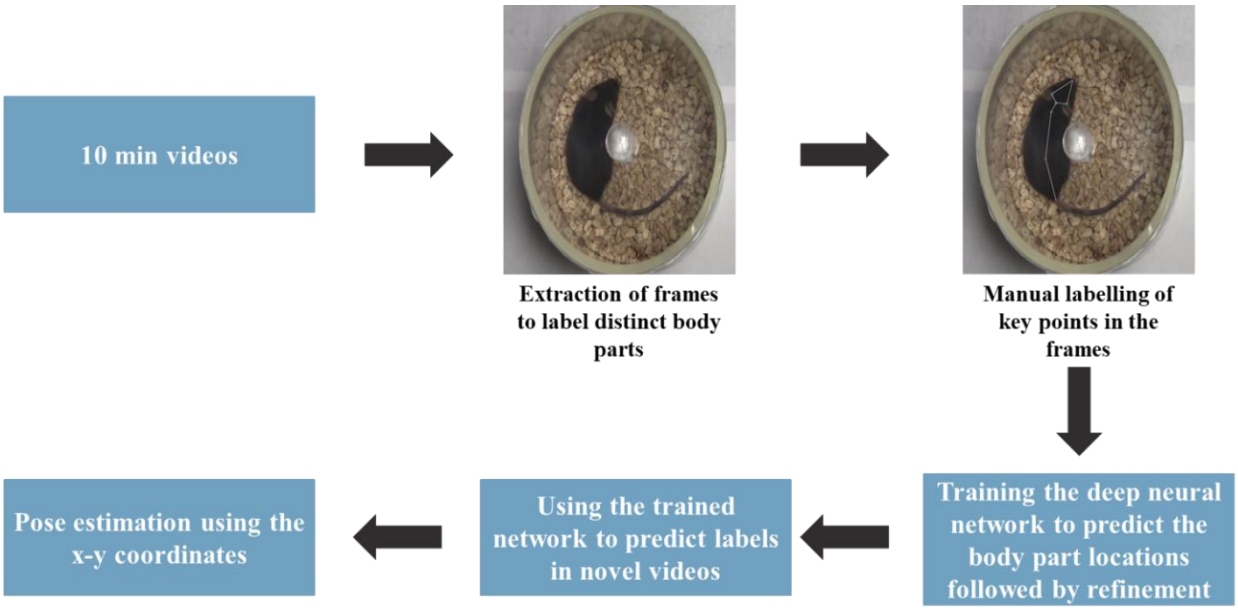

Figure 10 Workflow for video analysis using Deeplabcut.
(Images from our training set. The frames have been labelled for 7 key body parts.)

a. Data acquisition and pre-processing

For data acquisition and subsequent analysis, all behavioural sessions including the habituation and odour exposure days were recorded when the animal was placed inside the experimental chamber using a Canon LEGRIA HF R106 HD PAL Camcorder with 1440 × 1080 pixels resolution at 25 frames per second (fps). These videos were saved in MTS file format.

For further processing in DLC, all the videos were converted to an MP4 (or MPEG-4) file format using the FFmpeg library (About FFmpeg) in Python, without altering other aspects (frame rate, bit rate, etc.) of the videos.

b. Details of DLC model training and network validation

Initially, a total of 13 videos comprising a varied array of odour exposure experiments (PBS, AA and TMT exposure) recorded over a fairly large period of time were chosen to create an initial training set. Such a varied assortment was chosen to encompass a good mixture of camera angles and lighting conditions so that the model generalises well over novel videos.

For tracking, we extracted close to 20 distinct frames per video (based on k-means clustering method) from multiple experimental sessions in DLC. These frames were manually annotated for the nose point, left ear, right ear, and tail base. Further manual filtering to remove blurry or frames which did not have the mouse in the enclosure was also performed.

These annotated frames were used to train a ResNet-50 neural network with 500 epochs and a batch size of 1. During the entirety of the training, the data was randomly split into a training and a test set (95% (215 images) and 5% (12 images) respectively) to improve the efficiency of the model. In our case, since the initial model performance was sub-optimal, a second training set was undertaken (with 30 videos, batch size 8, 25 distinct frames per video, and an 85/15 training-test split for 500 epochs). Further, a 7-point skeleton system was created: to track nose point, left ear, right ear, mid ear point, anterior abdomen, posterior abdomen, and tail base. To validate the efficiency of the model over the course of the training, model error is calculated as the mean pixel distance (Root mean square error, RMSE) between human-annotated labels and network-predicted labels. The plot for the model error (in mm and pixels) over epochs for both cases is represented below (Figure 11). Further, representative images highlighting 7-point tracking as predicted by DLC (overlayed with human annotations) for test data set is also shown (Figure 12 a-d).

Although the second training set was slightly better than the first (mean error 5.16 mm; mean pixel error 32.23), its mean error at the end of 500 epochs was still 2.14 mm (mean pixel error 13.4 pixels). To further bring down the test error, a refinement training set was performed (with batch size 16 and until 500 epochs). During refinement, the wrongly predicted labels for novel videos and the annotations for 750 extracted frames were manually corrected (mean error 1.64 mm; mean pixel error 10. 24). Since the error for this set was the lowest, it was further utilised for tracking in the novel videos.

As an output, DLC yields a csv file with details of x-y coordinates in the space of all the predicted key points for novel videos. These co-ordinates could then be utilised for pose estimation using another neural network developed for behavioural prediction.

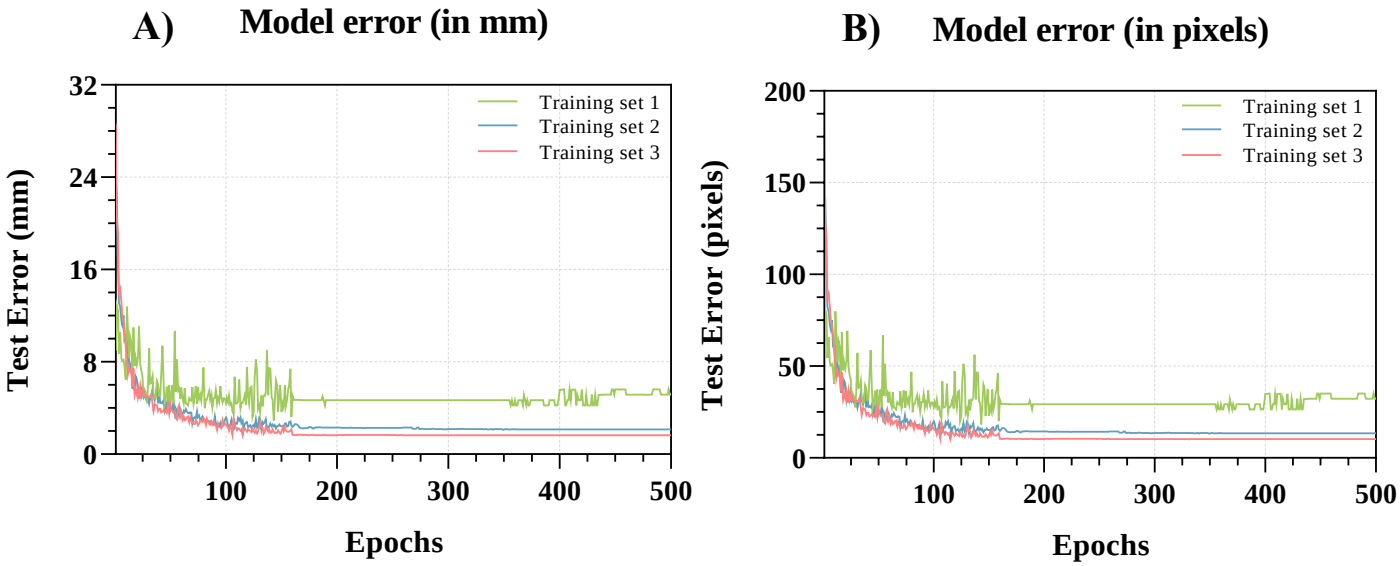

Figure 11 DeepLabCut model accuracy evaluation.
A shows the test error of the predicted labels during the training over epochs (number of iterations) in pixels whereas B shows it in mm. Mean RMSE for training set one is 5.16 mm; mean pixel error 32.23 px while for training set three is 1.64 mm and 10.24 pixels, respectively at the end of the training. Training set 3 (depicted in red) was utilised for all further analyses.

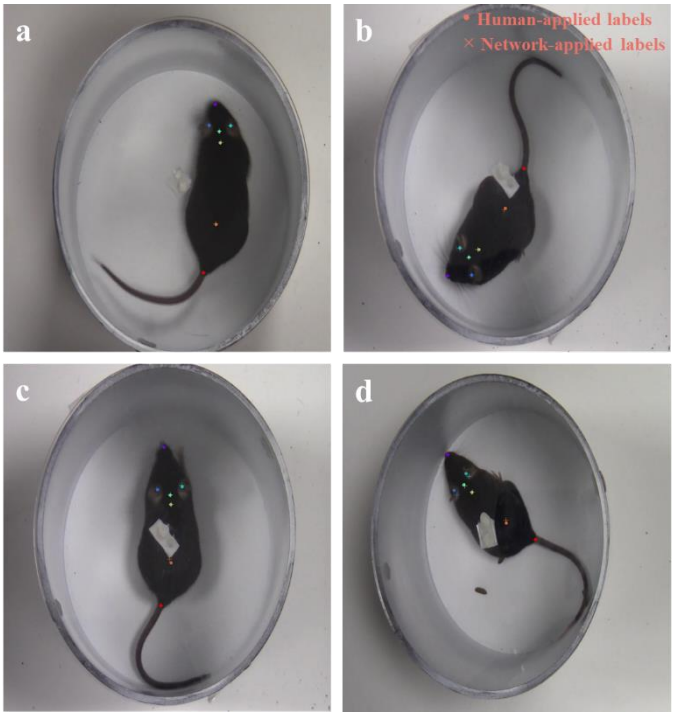

Figure 12 RMSE comparison between human-annotated and network-predicted labels.

a-d shows frames overlayed with network-applied labels (x) and human-applied labels (o) for the 7-key landmarks.

2.1.5.3. Behavioural annotation and prediction using SimBA (Simple Behavioural Analysis)

The behavioural videos for all sessions and their corresponding filtered DLC tracking data was fed into SimBA version 1.55 (Nilsson *et al.*, 2020; Goodwin *et al.*, 2024). No smoothening or interpolation was applied. To get a gist of scaling, the chamber width (13 cm) was utilised as a reference for calibrating the distance in the video to pixels per millimeter in the video, , resulting in an approximate value of 6.25 pixels per mm across all videos. In order to create a sufficiently robust model, a large number of videos encompassing several experimental sessions (and multiple groups of mice) were utilized. As our DLC neural network was satisfactory with lesser errors, outlier correction for creating behavioural classifiers was skipped in SimBA. Further, SimBA extracted a total of 26 features based on the filtered DLC tracking data. For behavioural classification, our training dataset included a total of 123 videos with 5sec-10 min duration, equating to 62,423 frames. Details for each behavioural classifier is listed in table below (table 1). In order to increase representations of rarely occurring behaviours (grooming and freezing), smaller clips ranging from 5s-300s were created to augment the training dataset in subsequent iterations.

Behaviours	No. of frames in the dataset	F1 score	Threshold
Exploration	35630	0.73	0.45
Grooming	26793	0.74	0.45
Freezing	16704	0.78	0.37

Table 1 Details of different behavioural classifiers utilsed for behavioural prediction.

Using the extracted features, DLC tracking data and manually annotated frames for different behaviours, we developed behavioural classifiers using a random forest model, an ensemble

learning method which classifies a behaviour based on majority of votes to a particular decision tree. The hyperparameters utilised to tune the model were: 2,000 estimators, a minimum leaf node of 1, RF_criterion set to "gini," RF_max_features set to "sqrt," and a test size of 20%.
Recognizing an imbalance in behavioural representation within the training data, we initially explored oversampling and undersampling. However, pilot tests revealed that the parameters lead to an increase in the efficiency of one parameter at the expense of the other, so we opted to forgo sampling modifications. Minimum bout durations were set at 500 milli seconds (ms) for exploration and freezing classifiers and 200 ms for grooming. To prevent behavioural overlap in the same frames, we applied a mutual exclusivity correction. If multiple behaviours were classified simultaneously, the one with higher probability of prediction would be preferred. The frames with equal probability were skipped from correction and were visually checked for the correct behaviour.

2.1.5.3.1 Accuracy Evaluation and Classifier Validation

Classifier performance was assessed using 20% of test frames from the entire training dataset, with accuracy reported as the F1 score—a harmonic mean of precision and recall that reflects classification reliability. Precision measures the proportion of true positive frames among all frames predicted as positive, while recall captures the proportion of true positives, among all the actual positives. Moreover, an important aspect of recall is that also accounts false negatives, which are essential for further refinement of the model.

$$Precision = \frac{TP}{TP + FP}$$

$$Recall = \frac{TP}{TP + FN}$$

$$F1 = 2 * \frac{Precision + Recall}{Precision * Recall}$$

To fine-tune classification accuracy, we determined discrimination thresholds—the probability at which a behaviour was classified as present—using Precision-Recall (PR) curves. These thresholds were optimized to maximize the F1 score, ensuring robust and reliable behaviour classification. Figure 13 below showcases the Precision-Recall (PR) curves utilized to create the behavioural classifiers.

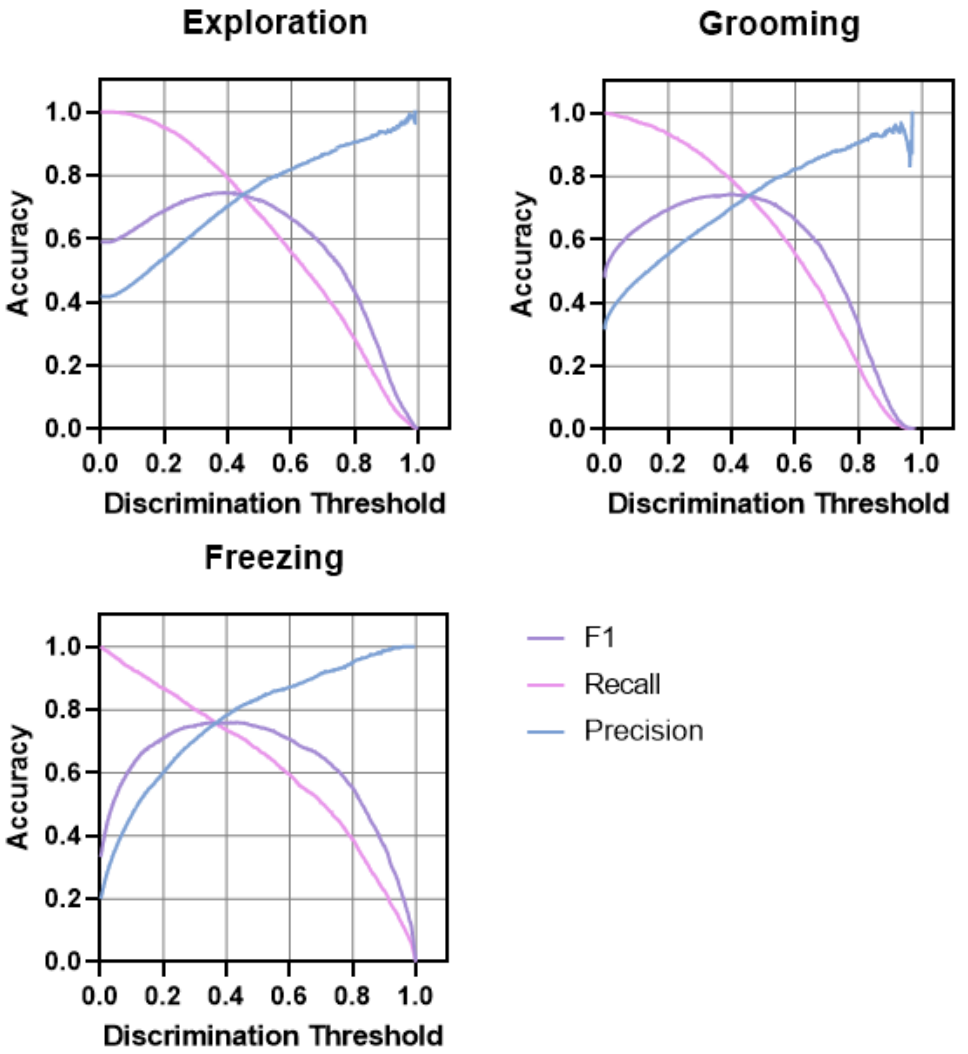

Figure 13 Precision Recall (PR) curves depicting the model accuracy for SimBA. For final analysis, thresholds were chosen such that F1 is maximised.

2.2 Behavioural characterization upon optogenetic modulation of the GAD65 interneurons

To delineate whether the threat perception and associated innate defensive responses could be modulated by a change in olfactory inputs, we utilised optogenetics. Retrograde labelling from the olfactory cortex to the bulb by previous studies have reported these inputs to be primarily glutamatergic (Wang *et al.*, 2024). Therefore, we proceeded with optogenetic modulation of GAD65 interneurons to discern their probable role in predator-odour processing.

2.2.1 Details of Stereotactic surgery and LED Implantation

For optogenetic modulation, all animals underwent cranial window surgery followed by LED implantation on the olfactory bulb upon attaining the experimental age. Detailed steps involved in the surgical process are outlined below (Figure 14):

a. Initially, each mouse is anaesthetized using an intraperitoneal injection of a combination of Ketamine and Xylazine solution (360:150). Anesthesia dosage is determined by the body weight of the animal – a mouse weighing in at 25g was administered ~50-60 µl of the anesthesia mixture (Ketamine: 50mg/g and Xylazine: 10mg/g).
b. Once the mouse is deeply anaesthetized (confirmed by loss of pedal reflexes upon toe-pinching), it is mounted on the stereotactic instrument using the ear and nose bars – which

support its zygomatic arches and snout respectively. To prevent the mouse's eyes from drying out, tear drops are applied over its eyes.

c. A circular cut is made to excise out a patch of the skin and fur overlying the olfactory bulb and the forebrain until lambda. The underlying connective tissue (periosteum) is thoroughly cleaned by scraping and cutting out using a fine, sharp scalpel.
d. Using a biopsy punch, a circular cranial window of 2.5 mm is etched over the olfactory bulb. Further, a dental drill bit is utilized to drill in a window along the etched marking in the cranium. The edges are smoothened and evened out to ensure that coverslip fits in snugly later. Next, using the scalpel, the drilled circular window is slowly lifted off the window to expose the underlying dura over the OB. The exposed area is cleaned with ACSF to clear off any blood spurting during this step.
e. An etching cream is then swiftly applied in the entirety of the exposed cranium (until lambda, posterior to intracranial vein). Using a q-tip it is swiftly wiped off following which a light-sensitive primer is applied.
f. The primer is UV-dried for 40s after which a small amount of tetric-N cream (white cement) is applied over the exposed cranium. Once again, a 40s cycle of UV exposure is applied.
g. Gently, a transparent, 3-mm round coverslip is lowered in the cranial window followed by a snug hold using the blunt-end of the Hamilton needle. A tiny, thin soft tissue is used to wipe off the extra-oozing CSF from the window.
h. A thin mixture of pink cement and dental cold-cure acrylic repair medium is utilized to firmly secure the coverslip in its place by applying it on its sides.
i. Further, the pink cement mix is applied to the entire exposed cranium to create a firm implant. It is allowed to dry out completely for 5-10 minutes.
j. After allowing a recovery period of 4-5 days, the mice are once again anaesthetized (~20 µl of anesthesia mixture for a short duration) for LED implantation onto the coverslips. ChR2 mice were implanted with blue LEDs whereas amber-coloured LEDs were utilized for ArchGFP and EYFP groups.
k. After making an even groove for the LED in the pink cement by drilling, the LED along with its connector is securely placed onto the coverslip. Utilising the Hamilton needle for a secure hold, a thin layer of pink cement mixture is applied generously to cover the LED base and connector.
l. Once the cement dries off completely, the mouse is unmounted from the stereotactic instrument and replaced back to its home cage for recovery from the surgery.
m. As post-operative care, the mice cages were placed on a heating pad to prevent hypothermia. Further, all mice that underwent surgery were fed moistened chow and special feed for fast recovery from surgery.

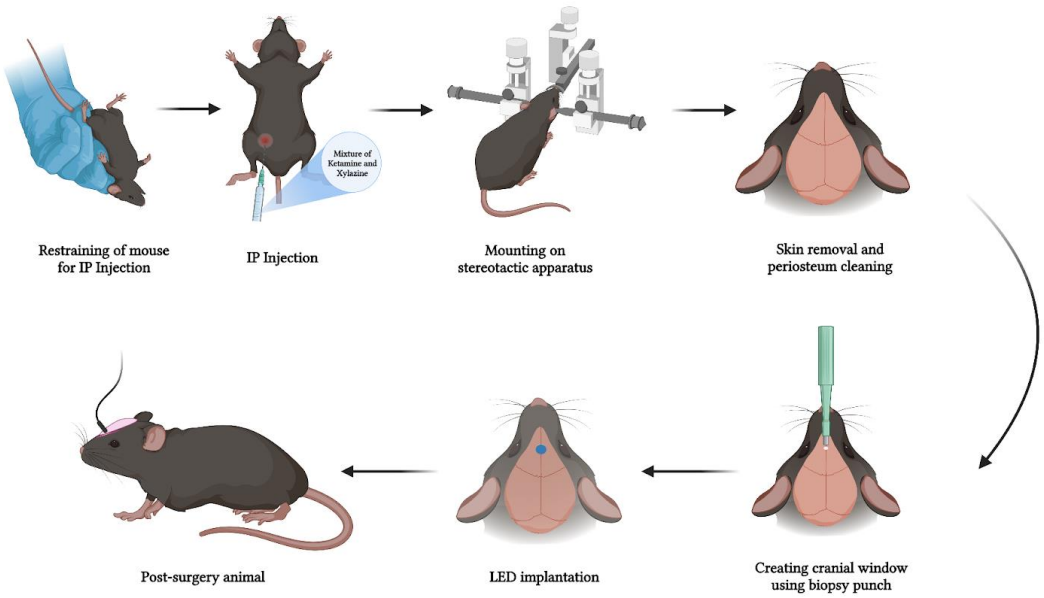

Figure 14 The stereotactic surgery procedure for LED implantation in freely-moving mice. Image courtesy: Debarghya De

2.2.2. Experimental Setup

All optogenetic experiments were also carried out in the same cylindrical-circular chamber (diameter and height = 13 cm). The lid however consisted of two perforations – one for the entry of odour delivery tube and the other smaller opening for the entry of the LED tether attached to the connecter at the mouse's head. Further, two small holes were made (3–4 cm below the brim of the chamber) which served as the passage for the exhaust tubing. During the experiments, the entire chamber was kept in a larger, opaque rectangular box to prevent any disturbance to the mice due to external surroundings.

To control precise and uniform odour delivery to the chamber, a small circuit with an Arduino Uno board, breadboard, pressure-pump, odour bottle, two odour valves, tubings, power supply and an LED driver was created. The circuitry was such that the Arduino board controlled a two-way pinch valve which would either deliver odour for 10 minutes (during the experimental session) or pump the odour in the exhaust tubing when the experiment was not running. These valves were connected after the odour bottle and a small, circular saturating ball for homogenous delivery of the odour. Another one-way valve was also used to serve as an airflow inlet into the chamber when the experiment was not running. This was done to flush out the residual odour in the chamber between sessions. The LED driver was used to control the LED intensity during the experiment. Further, a custom-written Arduino sketch was utilized to control the precise odour/airflow onset, and time and frequency of LED stimulation – 40 Hz stimulation for ChR2 and 1 Hz stimulation for Arch and EYFP. A power supply was utilized to power the Arduino board and the valves. A schematic representation illustrating the setup is attached in Figure 15.

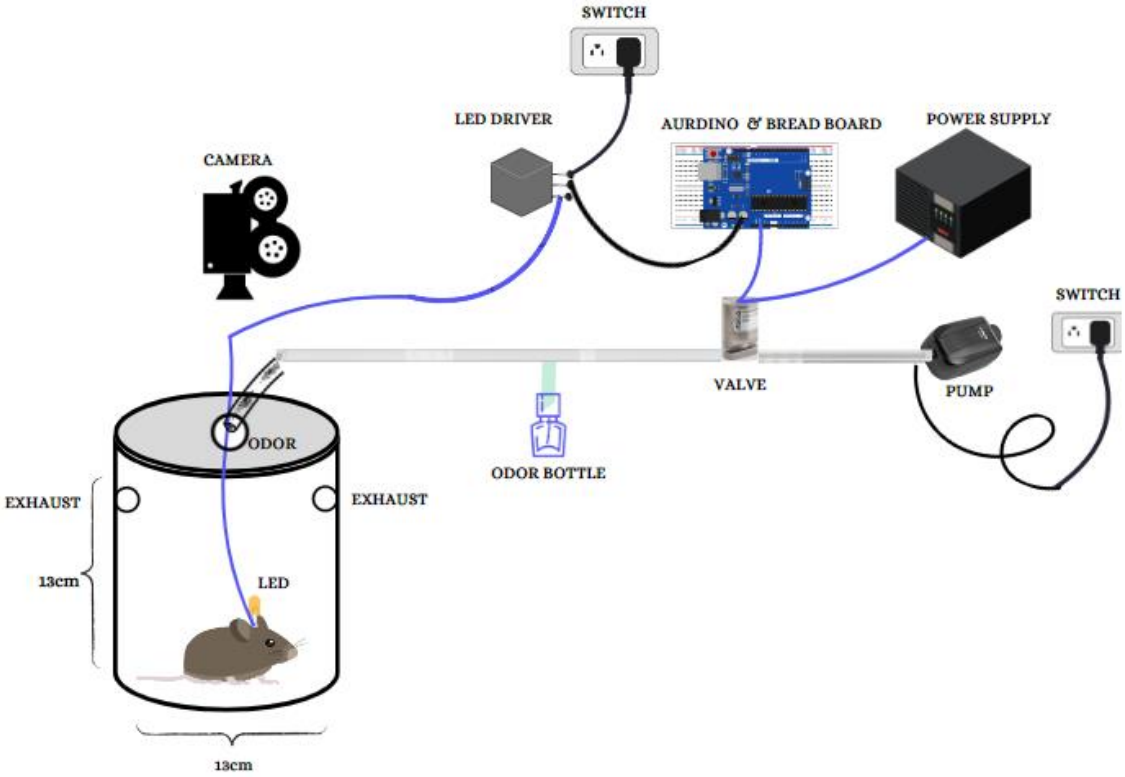

Figure 15 Schematic representation of the optogenetic setup.
Image courtesy: Sharvari Thorat

2.2.3. Experimental Timeline and Paradigm

To systematically characterize and modulate the activity of GAD65 interneurons in the processing of odours with either positive or negative valence, we recorded the behaviour of the mice in response to three different stimuli/odorants:

a. Airflow: a gentle continuous stream of air with which the odorants would later be introduced
b. AA odour: diluted 1% in mineral oil (v/v)
c. TMT odour: diluted 1% in 1x PBS (v/v)

The detailed paradigm is enumerated below and in Figure 16:

a. Habituation sessions

To negate the effects and any biases due to a novel arena, all mice were subjected to four consecutive sessions of habituation. During these sessions, the mice were introduced to the arena and were allowed to explore it for 10 minutes, after which they were replaced back to their homecage. During the last session, each of the mice was tethered to an LED connector which would later be utilized to power the LEDs implanted on them.

b. LED optimization sessions

To discern which particular light intensity should be utilized for the odour exposure sessions, we performed LED optimization. During this session, each mouse was once again tethered to the LED connector and subjected to a continuous exposure of 1% AA for 3 minutes. For each mouse we recorded – airflow, only odour and odour at three different light intensities (1.09 W, 3.496W and 4.888W for ChR2, and 0.72-5W for Arch). The light stimulation was adjusted to the different experimental groups (40 Hz stimulation for ChR2 and 1 Hz stimulation for Arch and EYFP) and was structured to be on for 5s and off for the next 3s for the entire duration of 3 minutes.

Further, after each of these 3-minute exposures, a 2-minute airflow delivery was provided in the chamber to flush out excess AA odour that might have accumulated in the chamber. The Arduino circuitry and the code ensured the precise odour and airflow delivery using a two-way pinch valve which would open at the beginning of the experiment to deliver odour for 3 minutes and automatically switch at the end of 3 minute-mark to deliver airflow for the next 2 minutes. This would then loop for at least 5 times to complete all exposure sessions for each mouse.

c. Airflow sessions

Post habituation, each mouse was further subjected to two sessions of airflow. During these airflow sessions, mice were tethered to the LED and placed in the chamber. During the first session, a continuous stream of airflow was provided for 10 minutes without any photo-stimulation. This was done to acclimatize the animal to the upcoming odorants which would also be accompanied with this flow rate.

During the second airflow session, a 10-minute airflow with photo-stimulation was provided. This was done to check for any impairment to the mobility/behaviour of the mice due to the photo-stimulation itself. The pulse structure for photo-stimulation was kept consistent for airflow and odour exposure sessions – 5s on and 3s off for 10-minute duration.

d. Odour exposure sessions

Similar to the airflow sessions, 4 odour exposure sessions were performed: AA with and without photo-stimulation and TMT with and without photo-stimulation. Briefly, mice were tethered to the LED connector and placed in the chamber, after which the lid was promptly closed. At this instant, odour delivery was turned on and photo-stimulation began with a delay of 5s when the odour possibly would have saturated the chamber. Each such session lasted for 10 minutes, after which the mouse was placed back to its home cage.

Further, during each of these sessions, mice were counter-balanced for a particular odorant group. That is, for TMT, half of the mice belonging to a particular sub-group underwent photo-stimulation on session, while the other half underwent photo-stimulation off on first session; and vice-versa for the second session. For, TMT sessions, care was taken that there was no/minimal pre-exposure to the odour before the actual session.

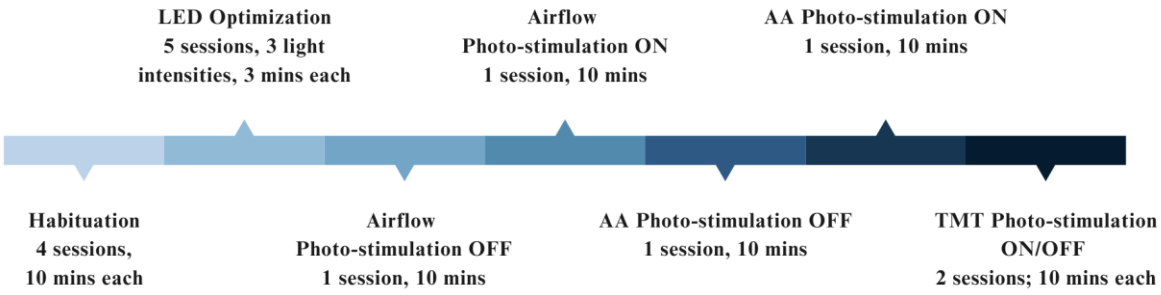

Figure 16 Paradigm illustrating the sequence of optogenetic sessions.

2.2.4. Behavioural analysis pipeline

For behavioural analysis, a similar pipeline to the behavioural characterization experiments is being followed: Bonsai analysis followed by DLC and SimBA analysis. Pilot results using Bonsai, which computes the change in Euclidean distance of the x-y coordinates of the mouse' centroid is shown in the respective results section.

Chapter 3 Results

3.1 Experiment 1: Behavioural characterization of ELS, NW, and ELS-EE mice

3.1.1. ELS mice present significantly higher anxiety-like behaviour compared to NW or ELS-EE mice

a. Elevated Plus Maze (EPM) Assay

To assess inherent anxiety states of the animals, EPM assay was carried out. Mice from the three cohorts – ELS, NW and ELS-EE were subjected to an elevated plus-shaped arena and allowed to explore for 5 minutes. Two of the arms in the arena are enclosed, while the other two open. Since rodents display a thigmotactic behaviour (tendency to prefer the walls or closed spaces), anxious individuals in such a scenario would exhibit more entries into the closed arms whereas less-stressed individuals would equally prefer both arms.

We computed the total number of entries into the open arm (frequency) and proportion of time spent in open arms, termed as Preference Index. It is calculated as percentage of time spent in the open arms (O) over total time spent in both the arms (open (O) and closed (C)). Figure 17 below shows representative tracks, preference index, and frequency for ELS, NW and ELS-EE mice.

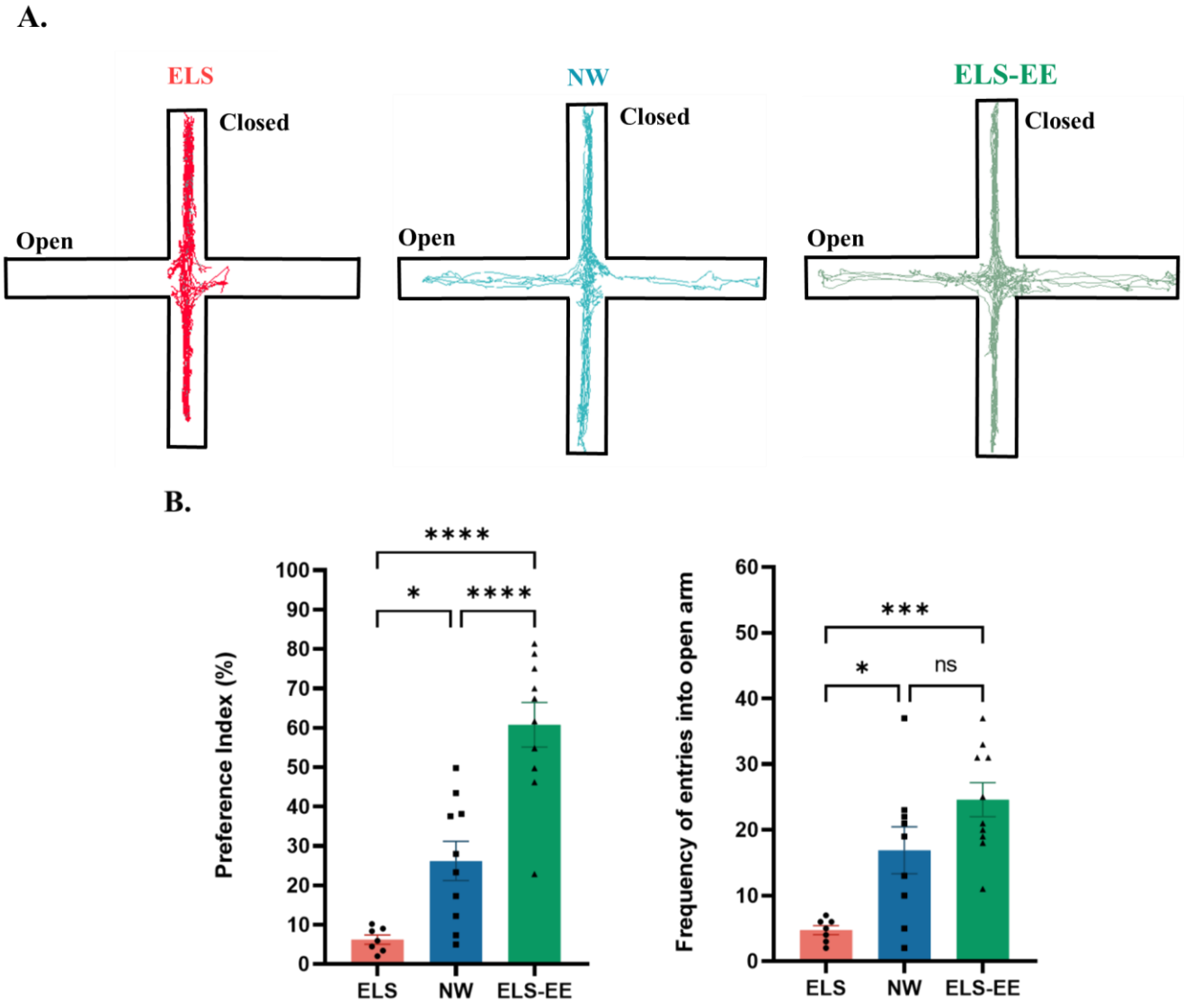

Figure 17 ELS mice present higher anxiety-like behaviour than NW or ELS-EE mice.
(A) Representative tracks undertaken by the three cohorts of mice during EPM assay.
(B) Preference index is plotted for the different categories of mice. ELS mice spend lower time in open arms as compared to NW or ELS-EE mice (ELS vs. NW, p = 0.0280; ELS vs. ELS-EE, p = <0.0001; NW vs. ELS-EE, p = <0.0001).

ELS mice further make fewer entries into the open arms compared to other two cohorts (ELS vs. NW, p = 0.0186; ELS vs. ELS-EE, p = 0.0002; NW vs. ELS-EE, p = 0.1219).
*Symbols represent individual mice (n =7 for ELS and n=9-10 for NW and ELS-EE). Bar and whiskers represent mean and s.e.m., respectively. * represent p < 0.05, **p < 0.01, ***p < 0.001, ****p < 0.0001, NS not significant - Ordinary one-way ANOVA with Tukey's multiple comparisons test.*

As observed ELS mice have a relatively lower frequency of entries into the open arms (mean frequency = 4.714), in comparison to NW and ELS-EE groups (mean frequency = 16.889 and 24.6 for NW and ELS-EE respectively). Further the preference index of ELS mice (mean percentage = 6.208) as indicated by percentage of time spent in open arms is significantly lower than NW (mean percentage time =26.192) and ELS-EE mice (mean percentage time =60.785). Both of these collectively indicate that the inherent anxiety levels in the three groups are significantly different, and ELS mice seem to experience relatively higher levels due to the chronic stress induced by early weaning paradigm.

3.1.2. Early-life stress affects predator-odour induced immobility in mice

To characterise the mobility of the animal upon TMT exposure, we utilised the open-source software Bonsai. The total time (in 10 minutes duration recorded at 25 fps, i.e., 15,000 frames) in which the animal was in mobile or stationary state is represented below in Figure 18 (n=4 (ELS), n=8 for NW and ELS-EE mice in each group. As visualized, the total amount of time spent mobile is relatively higher for the ELS group (496.46 sec) than the NW (434.55 sec) and EE group (425.61 sec), respectively. Further, ELS-EE (189.89 sec) mice have a relatively higher stationary time than both NW (178.105 sec) and ELS (127.98 sec) mice.

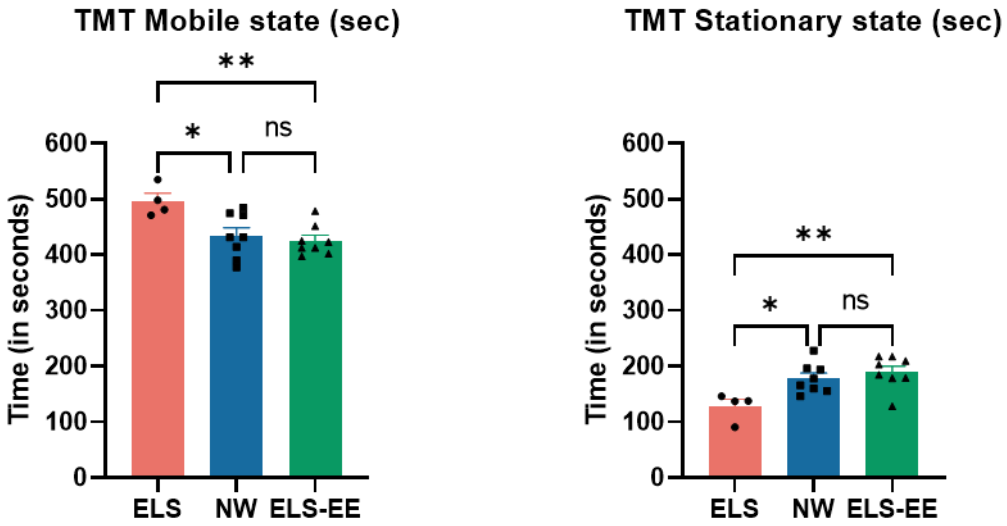

Figure 18 ELS affects predator-odour induced immobility in mice.
The mobile time for ELS mice is relatively higher (ELS vs. NW, p = 0.0238; ELS vs. ELS-EE, p =0.0056; NW vs. ELS-EE, p= 0.6808) while their stationary time is relatively lower (ELS vs. NW, p = 0.0188; ELS vs. ELS-EE, p = 0.0074; NW vs. ELS-EE, p = 0.8528).
*Symbols represent individual mice (n=4 (ELS), n=8 for NW and ELS-EE). Bar and whiskers represent mean and s.e.m., respectively. * represent p < 0.05, **p < 0.01, ***p < 0.001, ****p < 0.0001, NS not significant - Ordinary one-way ANOVA with Tukey's multiple comparisons test.*

Representative tracks for all three sets of mice are attached in Figure 19. Panel A, B and C show tracks for representative NW, ELS, and ELS-EE mice respectively. As visualized, tracks are denser for ELS mice than NW and ELS-EE mice, indicating that early-life stress leads to lesser freezing, and thus, modulates the innate defensive responses.

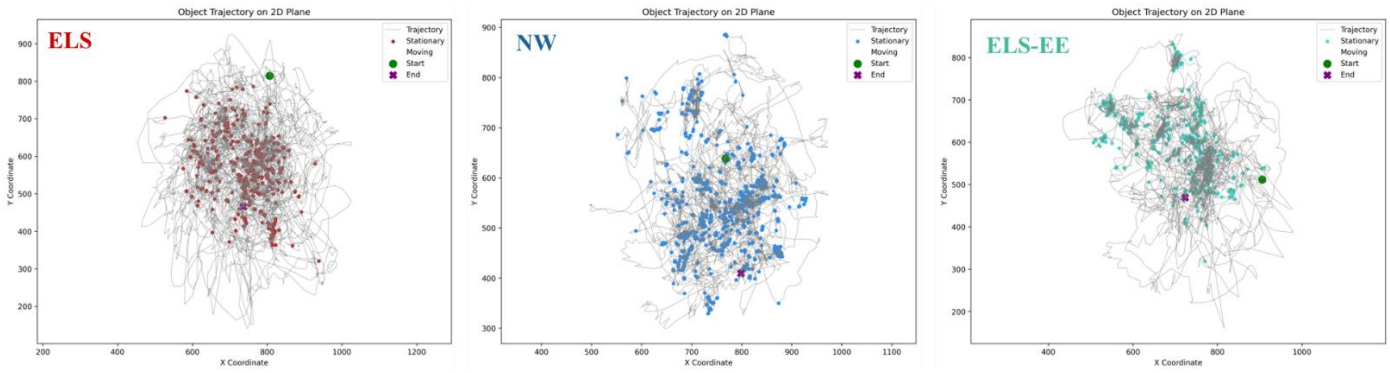

Figure 19 Representative tracks taken by ELS, NW and ELS-EE mice, respectively.

Axes represent the x-y coordinates of the centroid of mouse in space. Gray represents the trajectory taken by the mouse while each coloured dot represents one stationary episode in the path.

3.1.3 Early-life stress leads to a reduction in defensive behaviour

To further understand the nuances of the behavioural differences in the three cohorts of mice to different odour stimuli (PBS, AA and TMT), we utilized DeepLabCut and SimBA for markerless tracking, pose-estimation, and behavioural annotation of the mice. Three different behaviours were quantified: exploration, grooming and freezing. A brief description of these behaviours is enumerated below:

a. Exploration: refers to the unrestricted movement of mice in an arena. Mice tend to actively explore the arena for any novel stimulus by moving about or engaging in rearing behaviour – stretching their head upwards without any support from the walls of the enclosure (Chanthongdee *et al.*, 2024).
b. Self-grooming: comprises a patterned, sequence of actions such that the mouse initially performs elliptical bilateral strokes (using both paws) near its nose (paw and nose grooming), followed by unilateral paw strokes near its eye, succeeded by bilateral paw strokes (head grooming). Eventually, it progresses to cephalocaudal licking (body grooming). Further, grooming is believed to be an indicative of relaxed state in mice. (Spruijt *et al.*, 1992; Kalueff *et al.*, 2016).
c. Freezing: indicates a passive defensive response elicited against threatening stimuli. The mouse tends to take a crouched position with the cessation of all bodily movements except respiration (Fadok *et al.*, 2017).

For each cohort of mice, total time spent performing either exploration, grooming or freezing was normalised to the total time of the session, i.e., 600 seconds (10 minutes). These are illustrated below as normalized event duration (%) in figure 20, 21, and 22, respectively. Outlier correction was performed by calculating mean ± 2SD for all the datasets, and excluding all data points that did not fall within the criteria. All data is presented as the mean ± s.e.m.

In the case of ELS mice (Figure 20), we observe an increase in the duration of freezing from PBS to TMT ($p = 0.0282$) and AA to TMT ($p = 0.0118$), indicating these TMT acts as a threatful stimulus and elicits defensive responses. Further, there is no significant difference in the time spent in exploration and grooming across different experimental conditions. This implies that their overall mobility in the three conditions is similar.

In the case of NW mice (Figure 21), we observed an increase in the time spent in freezing from AA to TMT indicating that TMT might be perceived as a threat stimulus. However, in all other

cases – there seems to be no significant difference in their behaviour in different experimental conditions.

For ELS-EE (Figure 22), although there is an increase in their exploration time in the TMT exposure session conditions, we also observe a significant rise in their freezing time from PBS to AA and TMT. Further, there is also a mild drop in their grooming from PBS to TMT indicating their fear response.

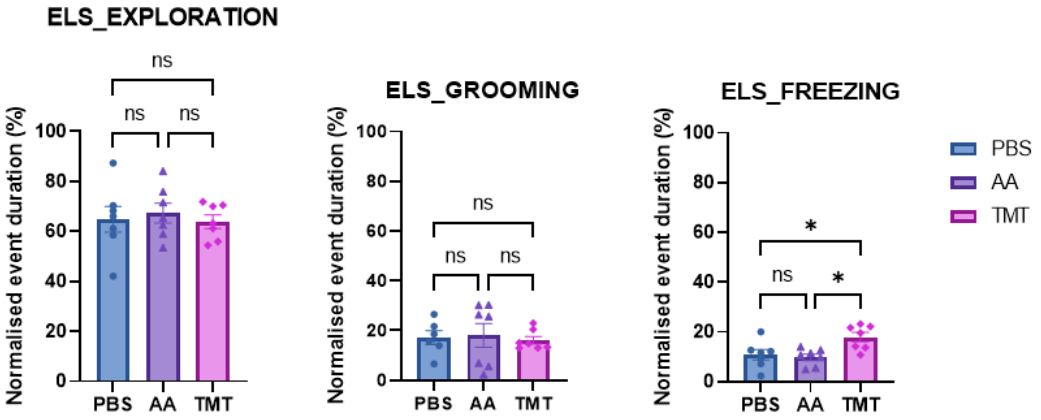

Figure 20 Predator-odour TMT brings about freezing in ELS mice.
Normalised duration of each behaviour (with respect to total duration of 600 seconds) is shown for ELS mice. The time spent in exploration or grooming is similar in all odorant conditions (PBS, AA and TMT). Exploration (PBS vs. AA, p = 0.9029; PBS vs. TMT, p = 0.9854; AA vs. TMT, p = 0.8246); Grooming (PBS vs. AA, p = 0.9812; PBS vs. TMT, p = 0.9721; AA vs. TMT, p = 0.9040).
However, we observe an increase in freezing in response to TMT (PBS vs. AA, p = 0.9101, PBS vs. TMT, p = 0.0282; AA vs. TMT, p = 0.0118) indicating the threat situation emulated by it.
*Symbols represent individual mice (n=6-10 for all). Bar and whiskers represent mean and s.e.m., respectively. * represent p < 0.05, **p < 0.01, ***p < 0.001, ****p < 0.0001, NS not significant - Ordinary one-way ANOVA with Tukey's multiple comparisons test for all.*

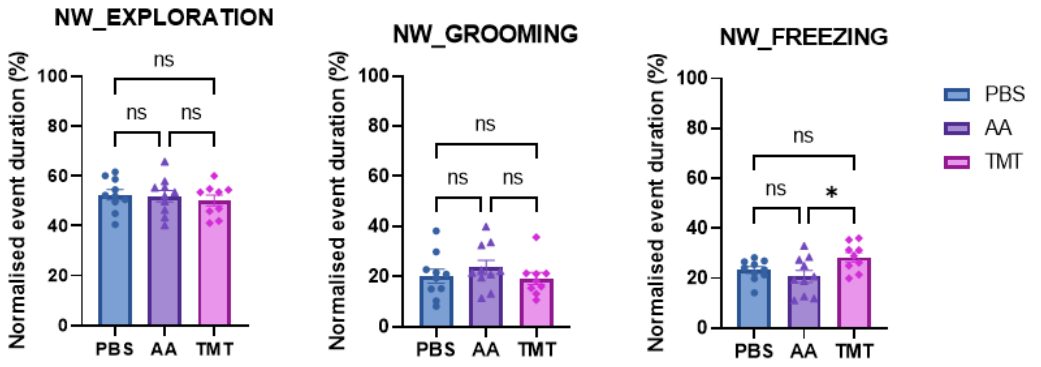

Figure 21 Predator-odour TMT brings about freezing in NW mice.
Normalised duration of each behaviour (with respect to total duration of 600 seconds) is shown for NW mice. The time spent in exploration or grooming is similar in all odorant conditions (PBS, AA and TMT). Exploration: PBS vs. AA, p = 0.9784; PBS vs. TMT, p = 0.7583; AA vs. TMT, p = 0.8630 and Grooming: PBS vs. AA, p = 0.6421; PBS vs. TMT, p = 0.9666; AA vs. TMT, p = 0.5051).
However, we observe an increase in freezing in response to TMT (PBS vs. AA, p = 0.6062; PBS vs. TMT, p = 0.1673; AA vs. TMT, p = 0.0245) indicating the threat situation emulated by it.
*Symbols represent individual mice (n=6-10 for all). Bar and whiskers represent mean and s.e.m., respectively. * represent p < 0.05, **p < 0.01, ***p < 0.001, ****p < 0.0001, NS not significant - Ordinary one-way ANOVA with Tukey's multiple comparisons test for all.*

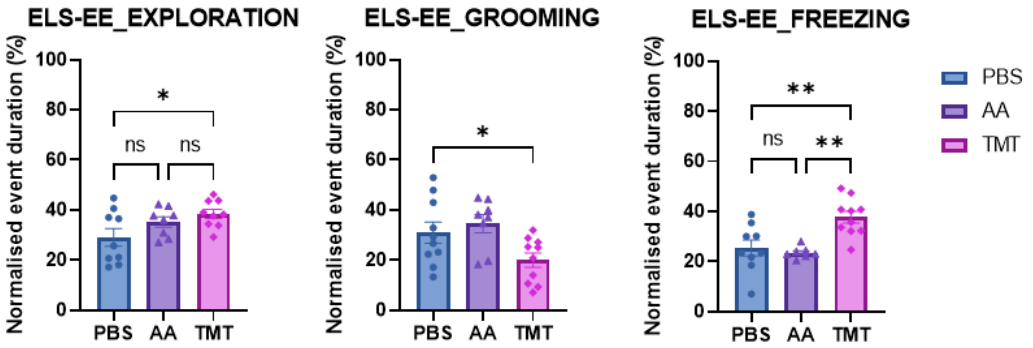

Figure 22 Effect of enrichment on different behaviours in ELS mice (ELS-EE).
Normalised duration of each behaviour (with respect to total duration of 600 seconds) is shown for ELS-EE mice. They show an increase in exploratory time (PBS vs. AA, p = 0.2647; PBS vs. TMT, p = 0.0443; AA vs. TMT, p = 0.6566, One-way ANOVA with Tukey's multiple comparisons test) while grooming mildly decreases (PBS vs. TMT, p =.0.0472, Unpaired t-test with Welch correction).
Further, we observe an increase in freezing in response to TMT (PBS vs. AA, p = 0.86; PBS vs. TMT, p = 0.0041; AA vs. TMT, p = 0.0020).
*Symbols represent individual mice (n=6-10 for all). Bar and whiskers represent mean and s.e.m., respectively. * represent p < 0.05, **p < 0.01, ***p < 0.001, ****p < 0.0001, NS not significant.*

An across group comparison (Figure 23) reveals that the time spent in exploration gradually decreases in both AA and TMT for the three cohorts of mice probably hinting at the innate differences in the exploratory nature of these mice.

Further, grooming in AA is significantly higher for ELS-EE mice in comparison to ELS and NW mice. Notably, ELS mice have a relatively lower duration of freezing in the case of TMT exposure, whereas NW and ELS-EE spent higher time in freezing. A similar trend is followed for AA as well.

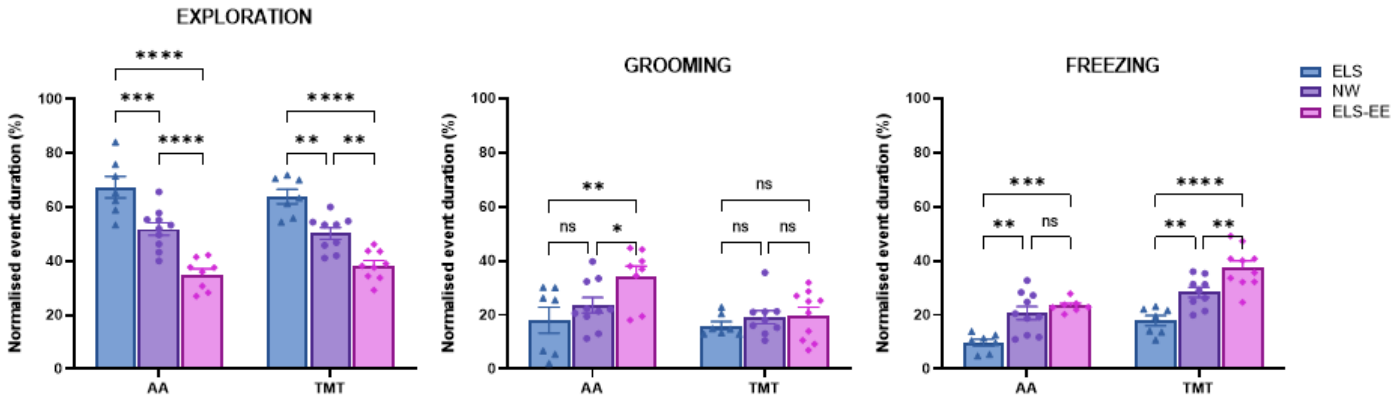

Figure 23 Comparision of all behaviours upon AA and TMT exposure for the three cohorts of mice.
Normalised duration of each behaviour (with respect to total duration of 600 seconds) is shown.
While exploration shows a significant decrease from ELS to NW and ELS-EE for both AA (ELS vs. NW, p = 0.0002; ELS vs. ELS-EE, p<0.0001; NW vs. ELS-EE, p<0.0001) and TMT exposure (ELS vs. NW, p = 0.0014; ELS vs. ELS-EE, p<0.0001; NW vs. ELS-EE, p = 0.0033), an increase in grooming is noted upon AA exposure in EE-ELS mice (ELS vs. NW, p = 0.4371; ELS vs. ELS-EE, p=0.0025; NW vs. ELS-EE, p = 0.0332).
Further, there is an increase in freezing from ELS to NW and ELS-EE for both AA (ELS vs. NW, p = 0.0014; ELS vs. ELS-EE, p<0.0002; NW vs. ELS-EE, p = 0.6205) and TMT exposure (ELS vs. NW, p = 0.0023; ELS vs. ELS-EE, p<0.0001; NW vs. ELS-EE, p = 0.6205), respectively.
*Symbols represent individual mice (n=6-10 for all). Bar and whiskers represent mean and s.e.m., respectively. * represent p < 0.05, **p < 0.01, ***p < 0.001, ****p < 0.0001, NS not significant - Mixed-effects analysis with Tukey's multiple comparisons test for all.*

This represents that upon TMT exposure, ELS mice exhibit higher mobility, while ELS-EE mice tend to exhibit higher defensive responses such as freezing (Freezing, Figure 23), thereby increasing their immobile time compared to NW. Previous studies have reported heightened stress responses in ELS mice due to dysregulation of the HPA axis, which eventually leads to elevated levels of the stress hormones like corticosterone in their blood serum. Elevated levels of corticosterone disproportionally activate the sympathetic nervous system, which brings about the physiological responses (Nishi, 2020). However, it remains unexplored whether such hyper-active responses are mounted due to relative differences in corticosterone in our case of ELS, NW and ELS-EE mice. To further delineate this, quantification of corticosterone levels in blood serum pre- and post-exposure to the predator odour TMT would be carried out in future.

3.1.4 ELS mice exhibit reduced neuronal activity in OB upon TMT exposure

To discern the neuronal activity in response to TMT, we visualised c-Fos, an immediate early gene which is synthesised post depolarisation, thereby serving as an indirect measure of neuronal activity (Bullitt, 1990).

All three cohorts of mice – ELS, NW and ELS-EE were subjected to the predator-odour TMT, following which three mice from each group were randomly chosen for c-Fos analysis in the olfactory bulb (OB) and amygdala. Figure 24 denotes a representative tile scan of the coronal section of the OB (using DAPI, a nuclear marker) to showcase the ROIs from where imaging was performed. For a uniform quantification across the OB, we took ROIs from the Dorsal (D), Medial (M), Lateral (L) and Ventral (V) regions of the Granule cell layer (GCL) of bulb.

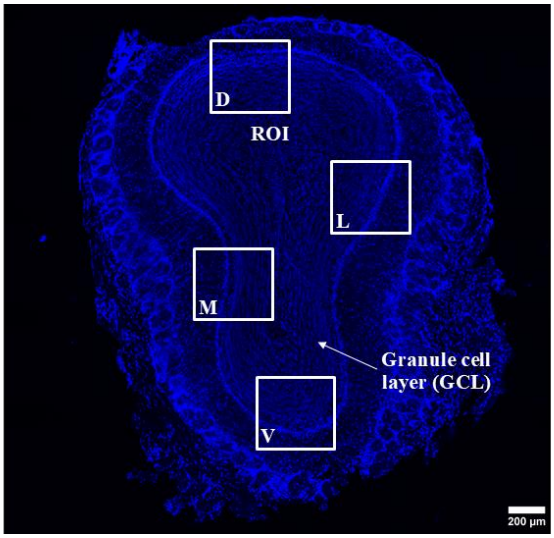

Figure 24 Representative coronal section of the mouse olfactory bulb showcasing distinct layered organization. 4 ROIs were chosen: Dorsal (D), Medial (M), Lateral (L) and Ventral (V) regions in the coronal section of the bulb. Blue represents DAPI staining. Scale bar: 200 µm

A large number of interneurons in the GCL of the OB were observed to be c-Fos positive suggesting their possible role in innate predator odour processing. The representative images for the early-life stressed (ELS), normally weaned (NW) and ELS-environmentally enriched (ELS-EE) groups upon TMT exposure are shown hereafter in Figures 25, 26 and 27, respectively.

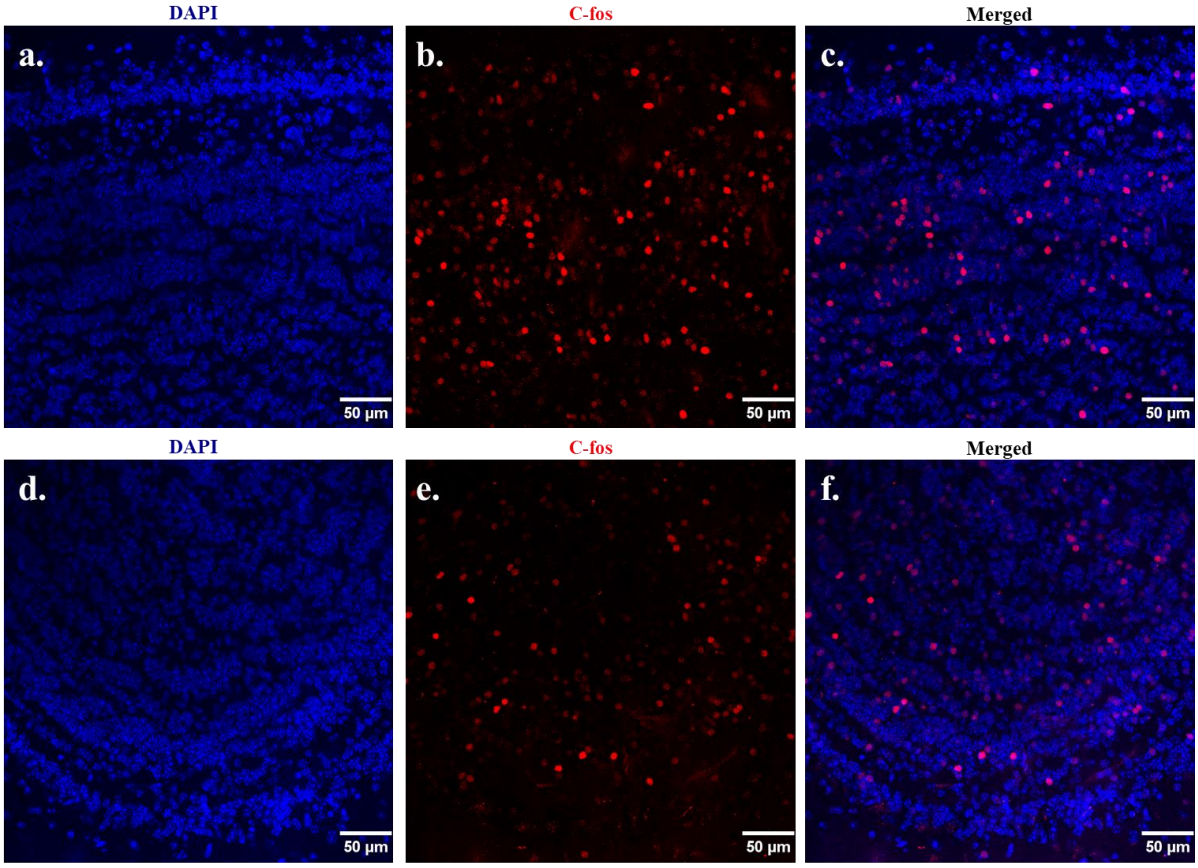

Figure 25 ***ELS:*** *Representative images showcasing c-Fos activity in the dorsal and ventral GCL. Granule cell layer (GCL) shows distinct cells expressing c-Fos marker. Dorsal GCL (a-c); Ventral GCL (d-f). a, d: DAPI, b, e: c-Fos, and c, f: a composite indicating cells positive for c-Fos in the GCL. Scale bar: 50 µm*

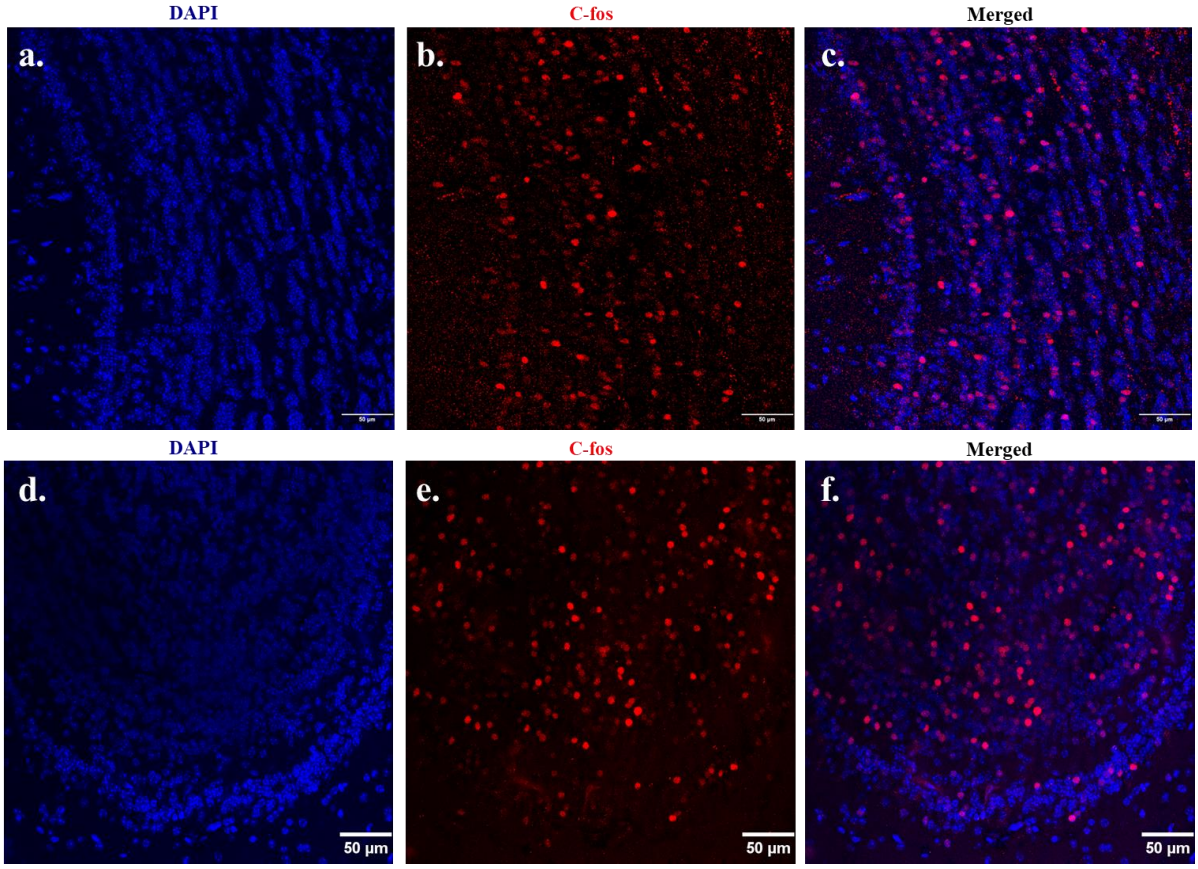

Figure 26 ***NW:*** *Representative images showcasing c-Fos activity in the lateral and ventral GCL.*

Granule cell layer (GCL) shows distinct cells expressing c-Fos marker. Lateral GCL (a-c); Ventral GCL (d-f). a, d: DAPI, b, e: c-Fos, and c, f: a composite indicating cells positive for c-Fos in the GCL. Scale bar: 50 µm

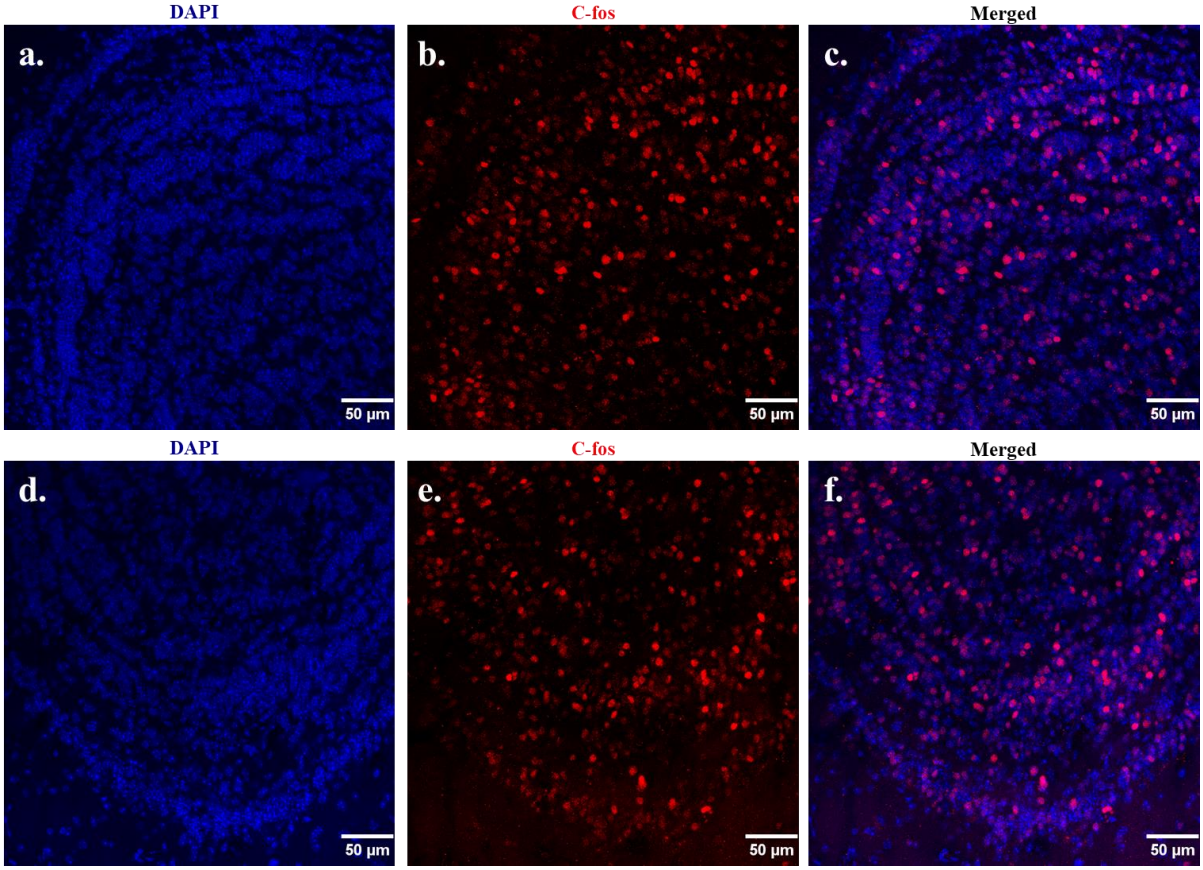

Figure 27 ***ELS-EE:*** *Representative images showcasing c-Fos activity in the dorsal and ventral GCL.*
Granule cell layer (GCL) shows distinct cells expressing c-Fos marker. Dorsal GCL (a-c); Ventral GCL (d-f). a, d: DAPI, b, e: c-Fos, and c, f: a composite indicating cells positive for c-Fos in the GCL. Scale bar: 50 µm

Quantification of the c-Fos positive cells across all three groups (Figure 28) revealed a significantly lower number of c-Fos positive cells in the ELS group in comparison to NW and ELS-EE groups, indicating a lower input from the OB to the higher cortical areas.

However, whether these differences in neuronal activity arise due to differential activation of interneurons in the OB of the three different groups, or due to cortical feedback to the bulb, remains unknown. Future experimentation in this regard would involve quantification of c-Fos positive cells in the amygdala to assess if the differences in bulbar input could also result in differential activity in the cortical areas.

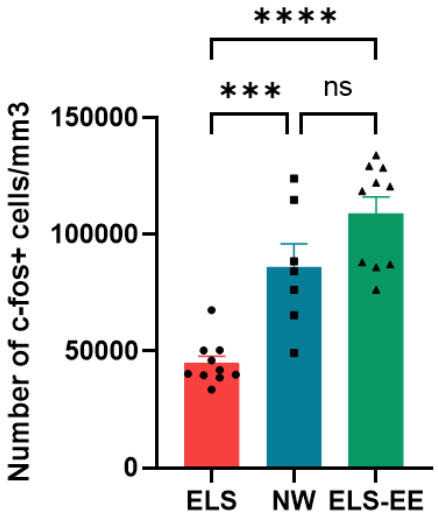

Figure 28 Lowered c-Fos activity in the GCL layer of olfactory bulb in ELS mice (cells/mm^3).
*Symbols represent average value across 3 mice (n=3, 7-10 ROIs for each mouse). Bar and whiskers represent mean and s.e.m., respectively. One-way ANOVA (with Tukey's multiple comparisons test) revealed a significant difference between the c-Fos positive cells in ELS versus NW or ELS-EE. (ELS-NW, p = 0.0008; ELS- ELS-EE, p<0.0001; NW-ELS-EE, p = 0.0647). *p < 0.05, **p < 0.01, ***p < 0.001, ****p < 0.0001, NS not significant.*

Further, tile scans denoting the overall pattern of neuronal activity in the OB for each of the three groups is shown below in Figure 29. Consistent with previous reports, we observe a larger activation in the dorsal and lateral regions (for NW), as compared to ventral OB (Kobayakawa *et al.*, 2007).

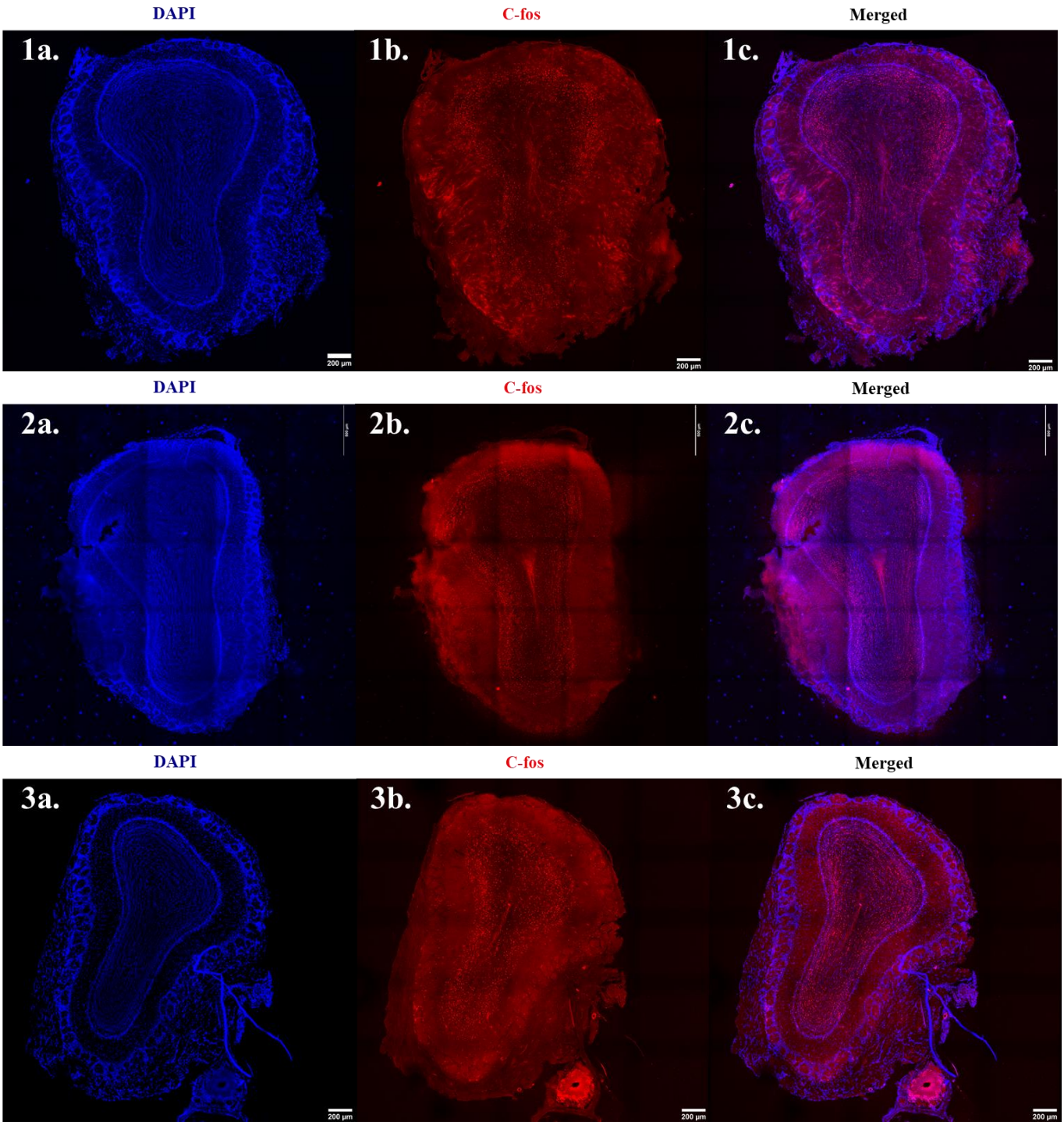

Figure 29 Tile scan of coronal sections exhibiting the broad neuronal activation in the GCL of the OB – for ELS, NW and ELS-EE mice.
ELS: 1a-c; NW: 2a-c; ELS-EE: 3a-c. a: DAPI, b: c-Fos, and c: a composite indicating cells positive for c-Fos in the GCL. Scale bar: 200 µm

3.2 Optogenetic modulation of the GAD65 interneurons in the olfactory bulb of ELS mice.

a. Increased synaptic inhibition in the OB of ELS mice increases mobility upon TMT exposure

To discern the underlying role of the olfactory inputs in mediating predator-odour induced defensive responses, we utilised optogenetics. Higher number of c-Fos positive cells were visualized in the Granule Cell Layer (GCL) of the olfactory bulb in response to TMT exposure. The GCL is abundantly known to harbour two kinds of interneurons – GAD65 (GAD2) positive and GAD67 positive interneurons. These interneurons are characterised by the presence of different isoforms of glutamate decarboxylase enzyme which brings about catalysis of glutamate to GABA. As previous reports have suggested a fairly higher abundance of GAD65 than GAD67, (78% of the total GAD population in rat OB) (Sheikh *et al.*, 1999; Parrish-Aungst *et al.*, 2007), we proceeded with optogenetic modulation of GAD65 interneurons in the bulb.

We utilised transgenic mice expressing opsins – either Channelrhodopsin-2 (ChR2), Archaerhodopsin (Arch) or, enhanced yellow fluorescent protein (EYFP) in the GAD65 interneurons of the OB. These three sub-groups of mice underwent early weaning, such that they would be stressed. These mice were further subjected to our experimental paradigm where they were exposed to airflow, AA and TMT sequentially. For each of these odorant conditions, we subjected them to two sessions of 10 minutes (600 seconds) each – a photo-activation on (denoted by light ON), and a photo-activation off session (denoted by light OFF).

Using Bonsai to track the mobility of the mouse, we calculated the time spent by the animal (in seconds, in 600 seconds) in stationary state in both photo-activation ON and OFF sessions. It is illustrated in Figure 30. Photo-activation in GAD-ChR2 animals would bring about activation of these interneuronal population thereby inhibition of the mitral cell output to the higher cortical areas. Further, photo-activation in GAD-Arch animals would bring about reduced inhibition in the OB due to inhibition of GAD65 interneurons. However, photoactivation in GAD-EYFP would not elicit any response, thus acting as a control for the presence of light during experiments.

Figure 30A demonstrates the effect of optogenetic modulation in GAD65-ChR2 group as compared to GAD65-EYFP. The normalised time (%) is calculated for all animals by calculating the percent of time spent in either stationary or mobile time over total time of the session. Outlier correction by exclusion of all data points that did not fall within mean ± 2SD was performed for all datasets. As observed, the stationary time for GAD-ChR2 mice is a bit lower than the EYFP group during the photo-activation ON session (Figure 30A), indicating that photo-activation of the GAD65 interneurons leads to a mild decrease in the freezing. No such difference is noted in the photo-activation OFF sessions, indicating the role of optogenetic modulation in bringing about these slight differences in the behaviour.

Figure 30B delineates the effects of optogenetic modulation in GAD65-Arch group as compared to GAD65-EYFP. However, no such difference is observed by modulation in the GAD65-Arch group in either photo-activation ON or OFF on both behavioural states. Further characterisation using the DLC-SimBA approach would offer a detailed snapshot into the behavioural states of the three groups of mice.

A. Stationary time (GAD-EYFP vs. GAD-ChR2

B. Stationary time (GAD-EYFP vs. GAD-Arch)

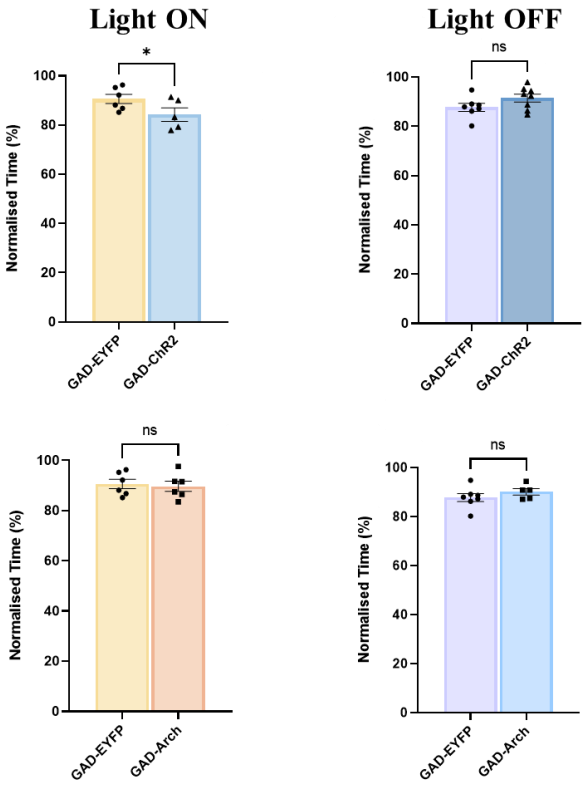

Figure 30 Effect of optogenetic modulation in GAD65-ChR2 and GAD-Arch groups as compared to GAD65-EYFP group, respectively.
A. Unpaired one-tailed t-test revealed a mild difference in the stationary time of the GAD-ChR2 mice in comparison to GAD-EYFP group (light on stationary time, p = 0.0398; light off stationary time, p = 0.0625).
B. Whereas, no difference in the stationary time is seen upon optogenetic modulation in the GAD-Arch group (light on stationary time, p = 0.3695; light off stationary time, p = 0.1613).
*Symbols represent individual mice (n=5-7 for all). Bar and whiskers represent mean and s.e.m., respectively. *p < 0.05, **p < 0.01, ***p < 0.001, ****p < 0.0001, NS not significant – Unpaired one-tailed t-test.*

Chapter 4 Discussion

In the current study, we aimed to understand if chronic stress could alter the threat perception and associated behavioural responses in ELS mice. Previously, multiple studies have reported impairments in cognitive tasks – such as decision-making (Jones *et al.*, 2009; Laino Chiavegatti and Floresco, 2024; Liu *et al.*, 2024) and working memory (Goodman *et al.*, 2019), and higher incidences of development of neuropsychiatric disorders (Karhina *et al.*, 2023; Tran and Gellner, 2023). However, whether its effects also manifest in innate behaviours, which are believed to be genetically hardwired, remains a question in the field. By utilising early weaning (EW) as a model of induction of chronic early life-stress, we attempted to bridge this gap by studying its effects on predator-odour induced defensive responses. These behaviours are induced against potential dangers in nature which decides the survival of the organism.

We began with three different cohorts of mice – an early-life stressed (ELS) group which were subjected to early weaning from post-natal day 14 (PND14), a normally weaned (NW) group weaned at PND 21, and a third group of mice (ELS-EE) which were subjected to ELS from PND 14-21 followed by environmental enrichment from PND21 until the experimental age of 6-8 weeks.

Each of these groups was subjected to three odour exposure conditions – PBS, AA and TMT. While we chose PBS as a neutral condition, AA and TMT, both have been demonstrated to carry a positive and negative valence, respectively for rodents (Root *et al.*, 2014). Behavioural analysis revealed that AA exposure brought about an increase in grooming behaviour from PBS to AA in NW and ELS-EE mice (although non-significantly different). This implies that exposure to a non-aversive odour brings about a relaxed state in mice (Root *et al.*, 2014). In all the three groups, TMT brought about a significantly higher amount of freezing (than PBS or AA) (Figures 20, 21 and 22). Freezing is a passive, innate defensive behaviour, which the animal elicits against predators. This indicates that TMT odour – which is a monomolecular component of the fox faeces, is sufficient to induce a threatful scenario, where the mice adopt a defense mechanism to maximise their survival. Previous studies which sought to study the functional value of freezing, have suggested that motionless prey have had a better chance at survival during a predator encounter than mobile individuals (Herzog and Burghardt, 1974). This could be explained by considering two reasons – for one, mammalian visual systems are tuned for detecting moving objects. Secondly, for most predators, movement serves as the key trigger for launching an attack (Fanselow *et al.*, 2019).

Further, as observed in Figure 23, both grooming and freezing seem to follow an increasing trend in AA exposure and TMT exposure sessions, respectively (from ELS to NW, and to ELS-EE). This might suggest that the odour perception for AA and TMT for ELS mice differs from NW and ELS-EE mice.

Fanselow and Lester's predator imminence continuum (Fanselow and Lester, 1988) (Figure 31) suggests that prey actively determine their defensive responses based on the perceived physical and psychological danger from the predator. This active selection of responses presents itself as a continuum, where on one end is the situation where the prey is the safest from the predator, and on the other end is the scenario where the predator kills the prey. At the lowest threat, the prey exhibits a change in its foraging, exploratory and meal patterns such that it could avoid contact with the predator. Moderate levels of threat (post-encounter) elicit freezing where the prey prioritizes avoiding any contact with the predator in the vicinity. Eventually, physical contact with the predator elicits the highest level of threat and such cases

draw aggressive fight-flight responses (Fanselow *et al.*, 2019; Fanselow, 2022). Low freezing and higher exploration in ELS mice upon TMT exposure could suggest that their perceived threat on the continuum could have shifted. A similar shift might have also caused higher freezing and lowered exploration in ELS-EE mice. However, what neural mechanisms bring about this shift, or if some other mechanism is at play, remain unknown.

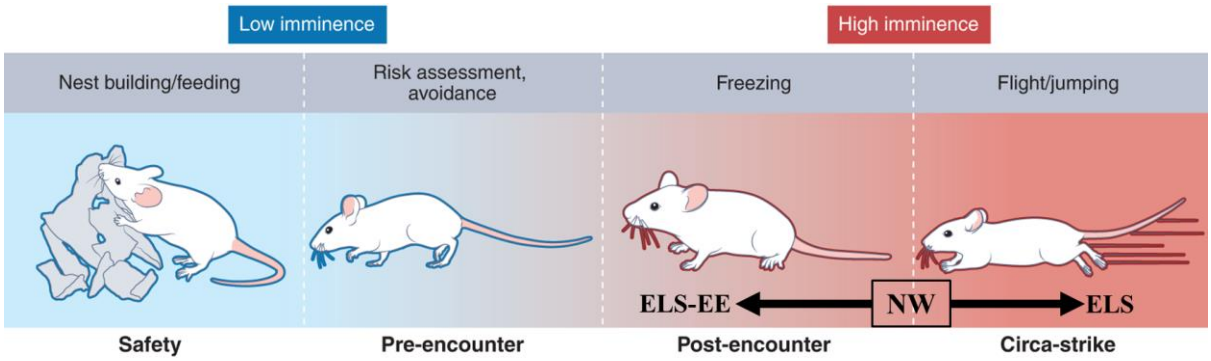

Figure 31 Shift in the defensive responses of ELS and ELS-EE mice.
While normally weaned (NW) mice can mount the right defensive response towards a threat, early weaning exacerbates the threat perception of mice leading to the induction of flight responses (ELS mice). Additionally, enrichment in ELS mice induces more freezing thereby altering their defensive responses too. Image adapted from (Moscarello and Penzo, 2022).

Further, c-Fos quantification (an indirect measure of neuronal activity) in the granule cell layer (GCL) of the olfactory bulb in response to TMT reveals a significantly lower number of inhibitory cells activated upon TMT exposure (Figure 28), possibly indicative of altered inhibition on the projection neurons in the OB, thereby affecting the odour perception.

Optogenetic activation of GAD65 inhibitory interneurons in the OB led to a mild decrease in the stationary time (Figure 30), indicating that photo-activation of GAD65 inhibitory interneurons might result in stronger odour-driven signals in M/T cells by altering the signal-to-noise ratio to the cortical centres. Further, given the inherent hyper-anxiety of the ELS mice, as evidenced by their reduced exploration in the EPM assay, their heightened threat perception could have led to the induction of flight responses. Photo-inhibition in GAD65-Arch animals did not present any significant behavioural differences as compared to GAD65-EYFP controls. This could be attributed to the idea that TMT elicits a stronger response in OB by activating a larger number of glomeruli in the dorsal and lateral OB (Kobayakawa *et al.*, 2007). Thus, it is likely that the extent of reduced inhibition by GAD65 interneurons in our experiments could not outweigh the minimum inhibition required for modulating the behaviour.

Further, a previous study by Pardasani et al. had also shown that ELS induces reduced synaptic inhibition on mitral/tufted (M/T) cells, which can manifest as cognitive deficits as their olfactory learning abilities are affected (Pardasani *et al.*, 2023). Our results present another dimension where we see that the ELS also affects innate defensive behaviours such as freezing.

Future experimentation and analyses

At the physiological level, previous studies have indicated that dysregulation of the HPA axis in the ELS mice could lead to prolonged, higher circulating levels of the ACTH and corticosterone (stress hormones). Further, both of these have been implicated in activating the sympathetic nervous system and thus leading to hyper-activity (Nishi, 2020; Lee and Jung, 2024). Further estimation of the corticosterone levels in our case needs to be carried out, to understand if this could be the underlying mechanism behind the behavioural differences in the

three sets of mice. In addition, a lot of local modulation on olfactory circuitry is exerted by neuropeptides such as corticotropin-releasing hormone (CRH), due to the presence of cognate-receptors of CRH on granule cells (Garcia *et al.*, 2016). Whether these neuropeptides also locally modulate the olfactory circuitry underlying the innate defensive behaviours remains unknown.

Moreover, it remains unknown whether the lowered activity in the GCL as visualised by c-Fos staining is due to low activation itself or due to cortical feedback to the olfactory inputs from the higher centres. To understand these, future experimentation would involve c-Fos quantification in the amygdala. Nevertheless, significantly higher mobility upon increasing inhibition suggests that the pre cortical circuitry indeed is not just a stimulus broadcasting centre but functions closely in adjunct with higher cortical areas to bring about different behavioural states, especially the predator odour driven freezing.

Lastly, most of our behavioural analyses were dependent on neural-network based model predictions. Therefore, it becomes important to further tune the model to pick up the minute nuances of the different rodent behaviours such as flight responses by quantification of jumps. In addition, further refinement of the model and slight tweaks in different hyper-parameters might lead to more efficient quantification of current behaviours.

References

Abaffy, T, Lu, H-Y, and Matsunami, H (2023). Sex steroid hormone synthesis, metabolism, and the effects on the mammalian olfactory system. Cell Tissue Res 391, 19–42.

Anderson, DJ, and Adolphs, R (2014). A Framework for Studying Emotions across Species. Cell 157, 187–200.

Barrios, AW, Núñez, G, Sánchez Quinteiro, P, and Salazar, I (2014). Anatomy, histochemistry, and immunohistochemistry of the olfactory subsystems in mice. Front Neuroanat 8, 63.

Bepari, AK, Watanabe, K, Yamaguchi, M, Tamamaki, N, and Takebayashi, H (2012). Visualization of odor-induced neuronal activity by immediate early gene expression. BMC Neuroscience 13, 140.

Blanchard, RJ, and Blanchard, DC (1989). Attack and defense in rodents as ethoexperimental models for the study of emotion. Progress in Neuro-Psychopharmacology and Biological Psychiatry 13, S3–S14.

Boccaccio, A, Menini, A, and Pifferi, S (2021). The cyclic AMP signaling pathway in the rodent main olfactory system. Cell Tissue Res 383, 429–443.

Bondar, NP, Lepeshko, AA, and Reshetnikov, VV (2018). Effects of Early-Life Stress on Social and Anxiety-Like Behaviors in Adult Mice: Sex-Specific Effects. Behavioural Neurology 2018, 1538931.

Brechbühl, J, Moine, F, Klaey, M, Nenniger-Tosato, M, Hurni, N, Sporkert, F, Giroud, C, and Broillet, M-C (2013). Mouse alarm pheromone shares structural similarity with predator scents. Proceedings of the National Academy of Sciences 110, 4762–4767.

Breton, JM, Cort, Z, Demaestri, C, Critz, M, Nevins, S, Downend, K, Ofray, D, Romeo, RD, and Bath, KG (2024). Early life adversity reduces affiliative behavior with a stressed cagemate and leads to sex-specific alterations in corticosterone responses in adult mice. Hormones and Behavior 158, 105464.

Bullitt, E (1990). Expression of C-fos-like protein as a marker for neuronal activity following noxious stimulation in the rat. Journal of Comparative Neurology 296, 517–530.

Carr, CP, Martins, CMS, Stingel, AM, Lemgruber, VB, and Juruena, MF (2013). The Role of Early Life Stress in Adult Psychiatric Disorders: A Systematic Review According to Childhood Trauma Subtypes. The Journal of Nervous and Mental Disease 201, 1007.

Chaby, LE, Sheriff, MJ, Hirrlinger, AM, and Braithwaite, VA (2015). Can we understand how developmental stress enhances performance under future threat with the Yerkes-Dodson law? Communicative & Integrative Biology.

Chanthongdee, K, Fuentealba, Y, Wahlestedt, T, Foulhac, L, Kardash, T, Coppola, A, Heilig, M, and Barbier, E (2024). Comprehensive ethological analysis of fear expression in rats using DeepLabCut and SimBA machine learning model. Front Behav Neurosci 18.

Chen, Y, and Baram, TZ (2016). Toward Understanding How Early-Life Stress Reprograms Cognitive and Emotional Brain Networks. Neuropsychopharmacol 41, 197–206.

Corbett, M (2015). From law to folklore: Work stress and the Yerkes-Dodson Law. Journal of Managerial Psychology 30, 741–752.

Efrat Jacob (2023). Differences in the Neurological Pathways of Innate and Learned Fear. The Science Journal of the Lander College of Arts and Sciences 17, 14–25.

Fadok, JP, Krabbe, S, Markovic, M, Courtin, J, Xu, C, Massi, L, Botta, P, Bylund, K, Müller, C, Kovacevic, A, *et al.* (2017). A competitive inhibitory circuit for selection of active and passive fear responses. Nature 542, 96–100.

Fanselow, M (2022). Negative valence systems: sustained threat and the predatory imminence continuum. Emerging Topics in Life Sciences 6.

Fanselow, MS, Hoffman, AN, and Zhuravka, I (2019). Timing and the Transition Between Modes in the Defensive Behavior System. Behav Processes 166, 103890.

Fanselow, MS, and Lester, LS (1988). A functional behavioristic approach to aversively motivated behavior: Predatory imminence as a determinant of the topography of defensive behavior. In: Evolution and Learning, Hillsdale, NJ, US: Lawrence Erlbaum Associates, Inc, 185–212.

Fendt, M, Brosch, M, Wernecke, KEA, Willadsen, M, and Wöhr, M (2018). Predator odour but not TMT induces 22-kHz ultrasonic vocalizations in rats that lead to defensive behaviours in conspecifics upon replay. Sci Rep 8, 11041.

Florido, A, Velasco, ER, Romero, LR, Acharya, N, Marin Blasco, IJ, Nabás, JF, Perez-Caballero, L, Rivero, G, Olabarrieta, E, Nuñez-delMoral, A, *et al.* (2024). Sex differences in neural projections of fear memory processing in mice and humans. Science Advances 10, eadk3365.

Fuentes, IM, and Christianson, JA (2018). The Influence of Early Life Experience on Visceral Pain. Front Syst Neurosci 12.

Fuss, SH, Omura, M, and Mombaerts, P (2005). The Grueneberg ganglion of the mouse projects axons to glomeruli in the olfactory bulb. European Journal of Neuroscience 22, 2649–2654.

Gallo, M, Shleifer, DG, Godoy, LD, Ofray, D, Olaniyan, A, Campbell, T, and Bath, KG (2019). Limited Bedding and Nesting Induces Maternal Behavior Resembling Both Hypervigilance and Abuse. Front Behav Neurosci 13.

Garcia, I, Bhullar, PK, Tepe, B, Ortiz-Guzman, J, Huang, L, Herman, AM, Chaboub, L, Deneen, B, Justice, NJ, and Arenkiel, BR (2016). Local Corticotropin releasing hormone (CRH) signals to its receptor CRHR1 during postnatal development of the mouse olfactory bulb. Brain Struct Funct 221, 1–20.

Ghosh, S, Larson, SD, Hefzi, H, Marnoy, Z, Cutforth, T, Dokka, K, and Baldwin, KK (2011). Sensory maps in the olfactory cortex defined by long-range viral tracing of single neurons. Nature 472, 217–220.

Giovanniello, JR, Paredes, N, Wiener, A, Ramírez-Armenta, K, Oragwam, C, Uwadia, HO, Yu, AL, Lim, K, Pimenta, JS, Vilchez, GE, *et al.* (2025). A dual-pathway architecture for stress to disrupt agency and promote habit. Nature, 1–10.

Goodman, JB, Freeman, EE, and Chalmers, KA (2019). The relationship between early life stress and working memory in adulthood: A systematic review and meta-analysis. Memory 27, 868–880.

Goodwin, NL, Choong, JJ, Hwang, S, Pitts, K, Bloom, L, Islam, A, Zhang, YY, Szelenyi, ER, Tong, X, Newman, EL, *et al.* (2024). Simple Behavioral Analysis (SimBA) as a platform for explainable machine learning in behavioral neuroscience. Nat Neurosci 27, 1411–1424.

Greer, PL, Bear, DM, Lassance, J-M, Bloom, ML, Tsukahara, T, Pashkovski, SL, Masuda, FK, Nowlan, AC, Kirchner, R, Hoekstra, HE, *et al.* (2016). A Family of non-GPCR Chemosensors Defines an Alternative Logic for Mammalian Olfaction. Cell 165, 1734–1748.

Gross, CT, and Canteras, NS (2012). The many paths to fear. Nat Rev Neurosci 13, 651–658.

Hacquemand, R, Jacquot, L, and Brand, G (2010). Comparative Fear-Related Behaviors to Predator Odors (TMT and Natural Fox Feces) before and after Intranasal ZnSO4 Treatment in Mice. Front Behav Neurosci 4, 188.

Hall, CS (1934). Emotional behavior in the rat. I. Defecation and urination as measures of individual differences in emotionality. Journal of Comparative Psychology 18, 385–403.

Hayakawa, S, Kataoka, K, Yamamoto, M, Asahi, T, and Suzuki, T (2024). DeepLabCut-based daily behavioural and posture analysis in a cricket. Biology Open 13, bio060237.

Herzog, HA, and Burghardt, GM (1974). Prey Movement and Predatory Behavior of Juvenile Western Yellow-Bellied Racers, Coluber constrictor mormon. Herpetologica 30, 285–289.

Imamura, F, Ito, A, and LaFever, BJ (2020). Subpopulations of Projection Neurons in the Olfactory Bulb. Front Neural Circuits 14.

Isosaka, T, Matsuo, T, Yamaguchi, T, Funabiki, K, Nakanishi, S, Kobayakawa, R, and Kobayakawa, K (2015). Htr2a-Expressing Cells in the Central Amygdala Control the Hierarchy between Innate and Learned Fear. Cell 163, 1153–1164.

Joëls, M, and Baram, TZ (2009). The neuro-symphony of stress. Nat Rev Neurosci 10, 459–466.

Jones, L, Yoon, T, and Kim, J (2009). Stress impairs decision-making in rats. Nat Prec, 1–1.

Kalueff, AV, Stewart, AM, Song, C, Berridge, KC, Graybiel, AM, and Fentress, JC (2016). Neurobiology of rodent self-grooming and its value for translational neuroscience. Nat Rev Neurosci 17, 45–59.

Karhina, K, Bøe, T, Hysing, M, and Nilsen, SA (2023). Parental separation, negative life events and mental health problems in adolescence. BMC Public Health 23, 2364.

Khalil, V, Faress, I, Mermet-Joret, N, Kerwin, P, Yonehara, K, and Nabavi, S (2023). Subcortico-amygdala pathway processes innate and learned threats. eLife 12, e85459.

Kobayakawa, K, Kobayakawa, R, Matsumoto, H, Oka, Y, Imai, T, Ikawa, M, Okabe, M, Ikeda, T, Itohara, S, Kikusui, T, *et al.* (2007). Innate versus learned odour processing in the mouse olfactory bulb. Nature 450, 503–508.

Laino Chiavegatti, G, and Floresco, SB (2024). Acute stress differentially alters reward-related decision making and inhibitory control under threat of punishment. Neurobiology of Stress 30, 100633.

Lara Aparicio, SY, Laureani Fierro, Á de J, Aranda Abreu, GE, Toledo Cárdenas, R, García Hernández, LI, Coria Ávila, GA, Rojas Durán, F, Aguilar, MEH, Manzo Denes, J, Chi-Castañeda, LD, *et al.* (2022). Current Opinion on the Use of c-Fos in Neuroscience. NeuroSci 3, 687–702.

Lauer, J, Zhou, M, Ye, S, Menegas, W, Schneider, S, Nath, T, Rahman, MM, Di Santo, V, Soberanes, D, Feng, G, *et al.* (2022). Multi-animal pose estimation, identification and tracking with DeepLabCut. Nat Methods 19, 496–504.

LeDoux, J (2012). Rethinking the Emotional Brain. Neuron 73, 653–676.

Lee, SH, and Jung, E-M (2024). Adverse effects of early-life stress: focus on the rodent neuroendocrine system. Neural Regeneration Research 19, 336.

Lezak, KR, Missig, G, and Carlezon Jr, WA (2017). Behavioral methods to study anxiety in rodents. Dialogues Clin Neurosci 19, 181–191.

Liu, Y, Wu, Y, and Yang, Q (2024). The impact of stress on the risk decision-making process. Psychophysiology 61, e14595.

Lopes, G, Bonacchi, N, Frazão, J, Neto, JP, Atallah, BV, Soares, S, Moreira, L, Matias, S, Itskov, PM, Correia, PA, *et al.* (2015). Bonsai: an event-based framework for processing and controlling data streams. Front Neuroinform 9.

Lopes, G, and Monteiro, P (2021). New Open-Source Tools: Using Bonsai for Behavioral Tracking and Closed-Loop Experiments. Front Behav Neurosci 15.

Ma, M, Grosmaitre, X, Iwema, CL, Baker, H, Greer, CA, and Shepherd, GM (2003). Olfactory Signal Transduction in the Mouse Septal Organ. J Neurosci 23, 317–324.

Mahajan, S, Tamboli, S, Das, S, Bhattacharjee, AS, Pardasani, M, Srikanth, P, Marathe, SD, Adlakha, A, Ranjan, L, Pandey, S, *et al.* (2024). Mouse olfactory system acts as anemo-detector and -discriminator. 2024.08.28.610087.

Malnic, B, Hirono, J, Sato, T, and Buck, LB (1999). Combinatorial Receptor Codes for Odors. Cell 96, 713–723.

Mamasuew, K, Breer, H, and Fleischer, J (2008). Grueneberg ganglion neurons respond to cool ambient temperatures. European Journal of Neuroscience 28, 1775–1785.

Marathe, SD, and Abraham, NM (2024). Synaptic inhibition in the accessory olfactory bulb regulates pheromone location learning and memory. 2024.09.08.611942.

Mathis, A, Mamidanna, P, Cury, KM, Abe, T, Murthy, VN, Mathis, MW, and Bethge, M (2018). DeepLabCut: markerless pose estimation of user-defined body parts with deep learning. Nat Neurosci 21, 1281–1289.

Matsukawa, M, Yoshikawa, M, Katsuyama, N, Aizawa, S, and Sato, T (2022). The Anterior Piriform Cortex and Predator Odor Responses: Modulation by Inhibitory Circuits. Front Behav Neurosci 16.

McEwen, BS, Bowles, NP, Gray, JD, Hill, MN, Hunter, RG, Karatsoreos, IN, and Nasca, C (2015). Mechanisms of stress in the brain. Nat Neurosci 18, 1353–1363.

Miyamichi, K, Amat, F, Moussavi, F, Wang, C, Wickersham, I, Wall, NR, Taniguchi, H, Tasic, B, Huang, ZJ, He, Z, *et al.* (2011). Cortical representations of olfactory input by trans-synaptic tracing. Nature 472, 191–196.

Morrow, BA, Redmond, AJ, Roth, RH, and Elsworth, JD (2000). The predator odor, TMT, displays a unique, stress-like pattern of dopaminergic and endocrinological activation in the rat. Brain Research 864, 146–151.

Moscarello, JM, and Penzo, MA (2022). The central nucleus of the amygdala and the construction of defensive modes across the threat-imminence continuum. Nat Neurosci 25, 999–1008.

Mueller, SC, Maheu, FS, Dozier, M, Peloso, E, Mandell, D, Leibenluft, E, Pine, DS, and Ernst, M (2010). Early-life stress is associated with impairment in cognitive control in adolescence: an fMRI study. Neuropsychologia 48, 3037–3044.

Nagayama, S, Homma, R, and Imamura, F (2014). Neuronal organization of olfactory bulb circuits. Front Neural Circuits 8, 98.

Nilsson, SR, Goodwin, NL, Choong, JJ, Hwang, S, Wright, HR, Norville, ZC, Tong, X, Lin, D, Bentzley, BS, Eshel, N, *et al.* (2020). Simple Behavioral Analysis (SimBA) – an open source toolkit for computer classification of complex social behaviors in experimental animals. 2020.04.19.049452.

Nishi, M (2020). Effects of Early-Life Stress on the Brain and Behaviors: Implications of Early Maternal Separation in Rodents. International Journal of Molecular Sciences 21, 7212.

Nishinaka, T, Nakamoto, K, and Tokuyama, S (2015). Enhancement of nerve-injury-induced thermal and mechanical hypersensitivity in adult male and female mice following early life stress. Life Sciences 121, 28–34.

Pantazopoulos, H, Dolatshad, H, and Davis, FC (2011). A Fear-Inducing Odor Alters PER2 and c-Fos Expression in Brain Regions Involved in Fear Memory. PLOS ONE 6, e20658.

Pardasani, M, Marathe, SD, Purnapatre, MM, Dalvi, U, and Abraham, NM (2021). Multimodal learning of pheromone locations. FASEB J 35, e21836.

Pardasani, M, Ramakrishnan, AM, Mahajan, S, Kantroo, M, McGowan, E, Das, S, Srikanth, P, Pandey, S, and Abraham, NM (2023). Perceptual learning deficits mediated by somatostatin releasing inhibitory interneurons of olfactory bulb in an early life stress mouse model. Mol Psychiatry 28, 4693–4706.

Parrish-Aungst, S, Shipley, M t., Erdelyi, F, Szabo, G, and Puche, A c. (2007). Quantitative analysis of neuronal diversity in the mouse olfactory bulb. Journal of Comparative Neurology 501, 825–836.

Root, CM, Denny, CA, Hen, R, and Axel, R (2014). The participation of cortical amygdala in innate, odor-driven behavior. Nature 515, 269–273.

Ryu, S, and De Marco, RJ (2017). Performance on innate behaviour during early development as a function of stress level. Sci Rep 7, 7840.

Sheikh, SN, Martin, SB, and Martin, DL (1999). Regional distribution and relative amounts of glutamate decarboxylase isoforms in rat and mouse brain. Neurochemistry International 35, 73–80.

Shonkoff, JP, Boyce, WT, and McEwen, BS (2009). Neuroscience, Molecular Biology, and the Childhood Roots of Health Disparities: Building a New Framework for Health Promotion and Disease Prevention. JAMA 301, 2252–2259.

Silva, BA, Gross, CT, and Gräff, J (2016). The neural circuits of innate fear: detection, integration, action, and memorization. Learn Mem 23, 544–555.

Smith, KE, and Pollak, SD (2020). Early life stress and development: potential mechanisms for adverse outcomes. J Neurodev Disord 12, 34.

Soares, JM, Sampaio, A, Ferreira, LM, Santos, NC, Marques, F, Palha, JA, Cerqueira, JJ, and Sousa, N (2012). Stress-induced changes in human decision-making are reversible. Transl Psychiatry 2, e131–e131.

Sosulski, DL, Bloom, ML, Cutforth, T, Axel, R, and Datta, SR (2011). Distinct representations of olfactory information in different cortical centres. Nature 472, 213–216.

Spruijt, BM, van Hooff, JA, and Gispen, WH (1992). Ethology and neurobiology of grooming behavior. Physiological Reviews 72, 825–852.

Takahashi, LK (2014). Olfactory systems and neural circuits that modulate predator odor fear. Front Behav Neurosci 8, 72.

Tian, H, and Ma, M (2004). Molecular Organization of the Olfactory Septal Organ. J Neurosci 24, 8383–8390.

Tran, I, and Gellner, A-K (2023). Long-term effects of chronic stress models in adult mice. Journal of Neural Transmission 130, 1133.

Tucker, LB, and McCabe, JT (2021). Measuring Anxiety-Like Behaviors in Rodent Models of Traumatic Brain Injury. Front Behav Neurosci 15.

Tyler, RE, Weinberg, B, Lovelock, D, Ornelas, L, and Besheer, J (2020). Exposure to the predator odor TMT induces early and late differential gene expression related to stress and excitatory synaptic function throughout the brain in male rats. Genes Brain Behav 19, e12684.

Wang, H, Wang, Q, Cui, L, Feng, X, Dong, P, Tan, L, Lin, L, Lian, H, Cao, S, Huang, H, *et al.* (2024). A molecularly defined amygdala-independent tetra-synaptic forebrain-to-hindbrain pathway for odor-driven innate fear and anxiety. Nat Neurosci 27, 514–526.

Wei, L, Simen, A, Mane, S, and Kaffman, A (2012). Early Life Stress Inhibits Expression of a Novel Innate Immune Pathway in the Developing Hippocampus. Neuropsychopharmacol 37, 567–580.

About FFmpeg. Available at: https://www.ffmpeg.org/about.html. Accessed October 15, 2024.